Journal of Orthopaedic Translation 35 (2022) 99–112

Contents lists available at ScienceDirect

Journal of Orthopaedic Translation

journal homepage: www.journals.elsevier.com/journal-of-orthopaedic-translation

Original article

Magnetic field therapy enhances muscle mitochondrial bioenergetics and attenuates systemic ceramide levels following ACL reconstruction: Southeast Asian randomized-controlled pilot trial

Mary C. Stephenson [a,1,***], Lingaraj Krishna [b,1], Rina Malathi Pannir Selvan [c,d], Yee Kit Tai [c,d,**], Craig Jun Kit Wong [c,d], Jocelyn Naixin Yin [c,d], Shi-Jie Toh [c,d], Federico Torta [e,f], Alexander Triebl [e], Jürg Fröhlich [g], Christian Beyer [h], Jing Ze Li [c], Sara S. Tan [b], Chun-Kit Wong [a], Duraimurugan Chinnasamy [i], Leroy Sivappiragasam Pakkiri [j,k], Chester Lee Drum [c,j,k], Markus R. Wenk [e,f], John J. Totman [a,l], Alfredo Franco-Obregón [c,d,m,n,o,p,*]

[a] Centre for Translational MR Research, Yong Loo Lin School of Medicine, National University of Singapore, Singapore
[b] Division of Sports Medicine and Surgery, Department of Orthopaedic Surgery, National University Hospital, National University Health System, Singapore
[c] Department of Surgery, Yong Loo Lin School of Medicine, National University of Singapore, Singapore
[d] BioIonic Currents Electromagnetic Pulsing Systems Laboratory, BICEPS, National University of Singapore, Singapore
[e] Singapore Lipidomics Incubator, Life Sciences Institute, National University of Singapore, Singapore
[f] Precision Medicine Translational Research Program, Department of Biochemistry, Yong Loo Lin School of Medicine, National University of Singapore, Singapore
[g] Fields at Work GmbH, Zurich, Switzerland
[h] Centre Suisse d'électronique et de Microtechnique, CSEM SA, Neuchatel, Switzerland
[i] National University Hospital, Department of Rehabilitation Centre, National University Health System, Singapore
[j] Cardiovascular Research Institute (CVRI), National University Heart Centre Singapore (NUHCS), Singapore
[k] Department of Medicine, Yong Loo Lin School of Medicine, National University of Singapore, Singapore
[l] Academic Radiology, Yong Loo Lin School of Medicine, National University of Singapore, Singapore
[m] Department of Physiology, Yong Loo Lin School of Medicine, National University of Singapore, Singapore
[n] Institute for Health Innovation & Technology, iHealthtech, National University of Singapore, Singapore
[o] NUS Centre for Cancer Research, Yong Loo Lin School of Medicine, National University of Singapore
[p] Competence Center for Applied Biotechnology and Molecular Medicine, University of Zürich, Zürich, Switzerland

ARTICLE INFO

Keywords:
Magnetic resonance
Metabolism
Mitochondria
Ligament reconstruction
Ceramides
Frailty biomarkers

ABSTRACT

Background: Metabolic disruption commonly follows Anterior Cruciate Ligament Reconstruction (ACLR) surgery. Brief exposure to low amplitude and frequency pulsed electromagnetic fields (PEMFs) has been shown to promote *in vitro* and *in vivo* murine myogeneses via the activation of a calcium–mitochondrial axis conferring systemic metabolic adaptations. This randomized-controlled pilot trial sought to detect local changes in muscle structure and function using MRI, and systemic changes in metabolism using plasma biomarker analyses resulting from ACLR, with or without accompanying PEMF therapy.

Methods: 20 patients requiring ACLR were randomized into two groups either undergoing PEMF or sham exposure for 16 weeks following surgery. The operated thighs of 10 patients were exposed weekly to PEMFs (1 mT for 10 min) for 4 months following surgery. Another 10 patients were subjected to sham exposure and served as controls to allow assessment of the metabolic repercussions of ACLR and PEMF therapy. Blood samples were collected prior to surgery and at 16 weeks for plasma analyses. Magnetic resonance data were acquired at 1 and 16 weeks post-surgery using a Siemens 3T Tim Trio system. Phosphorus (^{31}P) Magnetic Resonance Spectroscopy (MRS) was

* Corresponding author. Department of Surgery, Yong Loo Lin School of Medicine, National University of Singapore, NUHS Tower Block Level 8, 1E Kent Ridge Road, Singapore, 119228.
** Corresponding author. Department of Surgery, Yong Loo Lin School of Medicine, National University of Singapore, NUHS Tower Block Level 8, 1E Kent Ridge Road, Singapore, 119228.
*** Corresponding author. Centre for Translational MR Research, Yong Loo Lin School of Medicine, Tahir Foundation Building, 13-03, MD1, National University of Singapore, Singapore, 117549.
E-mail addresses: mary.stephenson@nus.edu.sg (M.C. Stephenson), surtaiyk@nus.edu.sg (Y.K. Tai), suraf@nus.edu.sg (A. Franco-Obregón).
[1] These authors contributed equally to the manuscript.

https://doi.org/10.1016/j.jot.2022.09.011
Received 30 May 2022; Received in revised form 23 September 2022; Accepted 24 September 2022
Available online 13 October 2022

utilized to monitor changes in high-energy phosphate metabolism (inorganic phosphate (P_i), adenosine triphosphate (ATP) and phosphocreatine (PCr)) as well as markers of membrane synthesis and breakdown (phosphomonoesters (PME) and phosphodiester (PDE)). Quantitative Magnetization Transfer (qMT) imaging was used to elucidate changes in the underlying tissue structure, with T1-weighted and 2-point Dixon imaging used to calculate muscle volumes and muscle fat content.

Results: Improvements in markers of high-energy phosphate metabolism including reductions in ΔP_i/ATP, P_i/PCr and (P_i + PCr)/ATP, and membrane kinetics, including reductions in PDE/ATP were detected in the PEMF-treated cohort relative to the control cohort at study termination. These were associated with reductions in the plasma levels of certain ceramides and lysophosphatidylcholine species. The plasma levels of biomarkers predictive of muscle regeneration and degeneration, including osteopontin and TNNT1, respectively, were improved, whilst changes in follistatin failed to achieve statistical significance. Liquid chromatography with tandem mass spectrometry revealed reductions in small molecule biomarkers of metabolic disruption, including cysteine, homocysteine, and methionine in the PEMF-treated cohort relative to the control cohort at study termination. Differences in measurements of force, muscle and fat volumes did not achieve statistical significance between the cohorts after 16 weeks post-ACLR.

Conclusion: The detected changes suggest improvements in systemic metabolism in the post-surgical PEMF-treated cohort that accords with previous preclinical murine studies. PEMF-based therapies may potentially serve as a manner to ameliorate post-surgery metabolic disruptions and warrant future examination in more adequately powered clinical trials.

The Translational Potential of this Article: Some degree of physical immobilisation must inevitably follow orthopaedic surgical intervention. The clinical paradox of such a scenario is that the regenerative potential of the muscle mitochondrial pool is silenced. The unmet need was hence a manner to maintain mitochondrial activation when movement is restricted and without producing potentially damaging mechanical stress. PEMF-based therapies may satisfy the requirement of non-invasively activating the requisite mitochondrial respiration when mobility is restricted for improved metabolic and regenerative recovery.

1. Introduction

The muscular mitochondrial compartment establishes systemic metabolic balance [1]. As such, post-surgical immobilization (silencing muscle) compromises systemic metabolic balance in association with depressed mitochondrial respiration [2], yet can occur independently of changes in muscle volume [3]. One manner in which muscle mitochondrial function influences whole-body metabolism is via actions of the muscle secretome [4]. In response to activity-dependent activation of mitochondrial respiration, skeletal muscle secretes into the systemic circulation a myriad of regenerative, inflammation and metabolic regulatory factors [4,5]. Accordingly, alterations in inflammatory cytokine levels have been observed following anterior cruciate ligament (ACL) injury [6] and subsequent surgical anterior cruciate ligament reconstruction (ACLR) [7].

The quadricep musculature is similarly adversely implicated by ACL injury [8], and reconstruction [9]. Despite recent advances in rehabilitation strategies, however, muscle weakness and atrophy can persist beyond 6 months of surgery [8,10]. Prolonged muscular impairment of this magnitude, besides increasing the risk of a recurrent injury [11], also undermines the ability of a patient to return to previous levels of physical activity [12], which will ultimately translate into metabolic disturbances with potentially long-term ramifications [13]. Losses of muscular mitochondrial content are also detectable for up to several years following chronically insufficient ACLR and is accompanied by depressions in oxidative muscle metabolic and physical capacities [14]. The development of therapeutic strategies to break this vicious degenerative cycle following ACLR surgery by sustaining mitochondrial function are urgently needed.

Physical inactivity correlates with muscular fat infiltration, mitochondrial dysfunction and systemic metabolic disruption. Post-trauma immobilization results in quadriceps adipose accumulation and is correlated with metabolic and cardiovascular disturbances [15]. ACLR is also characterized by fat infiltration that can persist up to a decade following surgery [16]. Immobilization-induced ectopic accumulation of adipose tissue into muscular and extramuscular sites is associated with increased circulating levels of toxic lipid metabolites, such as the palmitate-derived ceramides. Elevated muscle ceramide levels are associated with states of physical immobilization and sedentary lifestyles and are indicative of metabolic disturbances [17], whereas reductions in skeletal muscle ceramide levels are associated with improvements in systemic insulin sensitivity [18], and can occur independently of recovery from muscle atrophy [19]. Accordingly, elevated ceramide levels have been shown to undermine muscle maintenance and function as well as lead to metabolic and hepatic disturbances [20]. Importantly, certain long chain ceramide species have been shown to be toxic to mitochondria [20,21]. Notably, Tippetts et al. [21] recently provided evidence that blood ceramide levels may be a more precise predictor of cardiovascular disease and diabetes than cholesterol and underscored an unmet need for ceramide lowering therapeutics. The palmitate-derived lysophosphatidylcholines are also reputedly lipotoxic [22]. Elevations of lysophosphatidylcholine levels characterize sarcopenic muscle, wherein preventing its synthesis reinstates a youthful lipid profile, reduces metabolic stress, improves protein synthesis and promotes muscle recovery [23]. Lipotoxicity arising from elevated levels in ceramides species and lysophosphatidylcholine has also been shown to alter the gut microbiome resulting in metabolic dysfunction [22]. Paradoxically, the high caloric value of lipids also makes them the preferred mitochondrial energy substrate to sustain prolonged muscular activity. Heightened mitochondrial respiration, such as during aerobic training, recruits AMPK- and PGC-1α-dependent transcriptional pathways, stimulating *de novo* mitochondriogenesis and increasing mitochondrial fatty acid oxidation within skeletal muscle [24]. Consequently, intramyocellular lipid content has been shown to increase with aerobic training, predominantly in oxidative muscle characterized by elevated mitochondrial content and respiratory capacity [25]. Therefore, the accretion of lipids into skeletal muscle during changes in physical activity is context dependent; it is the inflammatory nature of the accumulated lipids, rather than absolute muscular lipid content *per se*, that drives systemic metabolic balance.

Magnetic Resonance Imaging and Spectroscopy (MRI, MRS) offers the capacity to investigate changes in muscle structure and metabolic status following ACLR. Their versatility allows for the measurement of muscle volumes, subcutaneous and intermuscular fat volumes [26], lipid content [27] and mitochondrial function [28] with which to ascertain therapeutic efficacy following ACLR. Combined, these distinct MRI/MRS modalities can provide a comprehensive overview of the muscular changes post ACLR.

Brief exposures to pulsed electromagnetic fields (PEMFs) were previously shown capable of promoting *in vitro* [29] and *in vivo* [30] murine

myogeneses via the activation of a calcium–mitochondrial axis promoting mitochondriogenessis, oxidative muscle maintenance, systemic metabolic balance, enhanced fatty acid oxidation as well as producing microbiome shift characteristic of leanness [30]. The implicated PEMF-induced calcium pathway pertained to that is mediated by the Transient Receptor Potential Canonical 1 (TRPC1) channel commonly implicated in load-bearing oxidative muscle development and is linked to PGC-1α transcriptional pathways underlying mitochondrial mitohormetic responses [30].

Here, we provide the results from a randomized-controlled pilot study employing a clinical prototype translated from earlier preclinical studies [29,30]. The pilot trial was conducted at the National University Health Systems (NUHS) of Singapore and authorized by the Domain Specific Review Board (DSRB) of the National Healthcare Group (NHG). The objective of the trial was to test whether brief (10 min) exposure to low amplitude (1 mT) pulsing magnetic fields administered on a weekly basis was capable of enhancing muscular mitochondrial function and systemic metabolic status as previously shown in our preclinical studies [29,30]. In this report, we provide initial indications that PEMF therapy holds the potential to promote muscle metabolism and improve healing following ACLR with as little as 10 min of exposure per week for a duration of 16 weeks. Most, notably we observed significant reductions in systemic ceramide levels that correlated with localized changes in markers of muscular mitochondrial function and phospholipid membrane breakdown in the operated limbs of patients receiving weekly PEMF therapy.

2. Materials and methods

We conducted a single-center, prospective, double-blinded, placebo-controlled, randomized-controlled trial with 1:1 allocation from March 2017 to January 2018. This trial was reviewed and approved by the National Healthcare Group Domain Specific Review Board, Singapore and registered on ClinicalTrials.gov (ClinicalTrials.gov number: NCT03165318). All patients gave written consent for the trial and were recruited from the National University Hospital (Singapore). The trial was conducted in accordance with the Good Clinical Practice guidelines and the principles of the Declaration of Helsinki. The trial specifics and inclusion and exclusion criteria are described in the **Supplementary Tables 1 and 2**

2.1. Participants

We calculated the sample size for difference of two means hypothesis testing. Setting a significance level of 5%, power of 80%, and effect size of 20%, the anticipated sample size is 22 participants. Block randomisation was performed at the time of recruitment via a web-based, blinded code list by an investigator who was not involved in the patient's clinical care. 22 patients meeting the above inclusion and exclusion criteria and requiring ACL reconstruction (ACLR) were recruited into the study and were randomized to receive PEMF or sham-exposure. Two patients chose to withdraw from the trial due to standing scheduling conflicts and time commitment to the study. All other patients exhibited 100% compliance to all procedures. Patients underwent a range of procedures including ACL Surgery, standard clinical rehabilitation, strength testing, blood analysis and clinical scoring as outlined in CONSORT diagram and patient schedule in Supplementary Tables 1 and 2

2.2. ACL reconstruction and rehabilitation

At surgery, standard medial and lateral arthroscopic portals were created adjacent to the patellar tendon, and diagnostic arthroscopy was performed to assess the ACL tear and concurrent injuries. A longitudinal skin incision of approximately 3 cm was then made on the anteromedial tibial surface at the level of the pes anserinus. The gracilis and semitendinosus tendons were identified and divided at their tibial insertion without elevation of the subperiosteal sleeve and harvested using a closed tendon stripper. A detailed description of the surgical procedure is provided in the Supplementary Methods; *Detailed Surgical Procedure*.

Postoperatively, all patients received appropriate analgesia and underwent a standard rehabilitation program per our institutional protocol. Patients were prescribed with early weight-bearing and range of motion exercises. Patients who underwent concomitant meniscal repair were restricted to 0–90 degrees of flexion for the first 6 weeks after surgery.

2.3. PEMF therapy

PEMF therapy was administered in conjunction with standard rehabilitation protocol using an in-house designed and contract-built apparatus delivering a time-variant magnetic signal previously optimized in murine muscle *in vitro* [29] and *in vivo* [30]. Briefly, 10-min exposures to 1 mT peak amplitude PEMFs were performed weekly on the operated thigh of patients post-ACLR for 16 weeks. Patients of the sham controls were treated identically to experimental patients, to ensure patient blinding, but no fields were administered. Special precautions were made to assure that participants were unaware of the operation of the device and to which experimental cohort they pertained. Most subjects are unable to perceive noise arising from the device during normal operation. The PEMF device prototype used in this trial was fabricated by XentiQ (Pte) Ltd (Singapore) according to the guidelines and specifications provided by the Department of Surgery, Yong Loo Lin School of Medicine of the National University of Singapore (NUS) (Fig. 1).

2.4. Muscle bioenergetics and membrane kinetics

MRI and MRS data were acquired using a Siemens 3T Tim Trio system located at the Clinical Imaging Research Centre (CIRC), National University of Singapore. To investigate muscle bioenergetics and membrane kinetics, phosphorus (31P) MRS data was acquired using a pulse-acquire sequence with the following parameters: TR = 12000 ms, BW = 3000Hz, No. points = 2048. A 60° flip angle rectangular pulse was used to optimize signal acquisition from the quadriceps. The region of interest monitored was the dorsal mid-thigh region. Specifically, the measuring coils were placed over the rectus femoris and the vastus muscles on the front of the thigh. A 1 mL bottle of methyl diphosphonic acid was positioned on the back of the coil to ensure coil position over quadriceps. ^{31}P MRS data were truncated to 512 points, zero-filled to 2048 points, and apodized (8Hz Lorentzian) before phase and frequency correction using jMRUI (jMRUI Consortium). The resulting spectra were fitted in AMARES [31]. Singlet Lorentzian peaks were fitted for phosphocreatine (PCr), the two phosphomonoesters (PMEs), phosphocholine (PCho) and phosphoethanolamine (PE), and the two phosphodiesters (PDEs), glycerophosphocholine (GPC) and glycerophosphoethanolamine (GPE). Adenosine triphosphate (ATP) was fitted as two doublets (gamma, and alpha) and a triplet (beta-moiety) with fixed linewidths and amplitude ratios across multiplets. Two single peaks were fitted for inorganic phosphate (Pi) to allow for potential acidification in one of the two (possible) compartments, typically seen during intense exercise. This second peak tended to be only a small contribution to the larger Pi peak, with its shift variable across subjects. As such, the second peak was included in the Pi concentrations but data for pH are presented with and without this second peak. PCr/ATP, P_i/ATP, P_i/PCr and (Pi + PCr)/ATP as well as pH were calculated to investigate bioenergetics, PDE/ATP and PME/ATP were calculated to investigate cellular membrane kinetics. Data are presented as percentage change from visit 1 with absolute change for in pH.

2.5. Muscle and tissue volumes

Muscle volumetrics were obtained using a T_1-weighted turbo spin-echo sequence with TE/TR = 13/600 ms, voxel size = 0.4 × 0.4 × 5mm^3, matrix = 512 × 512 × 32. Cross-sectional tissue and muscle volumes were calculated from a single slice at the mid-point of the thigh

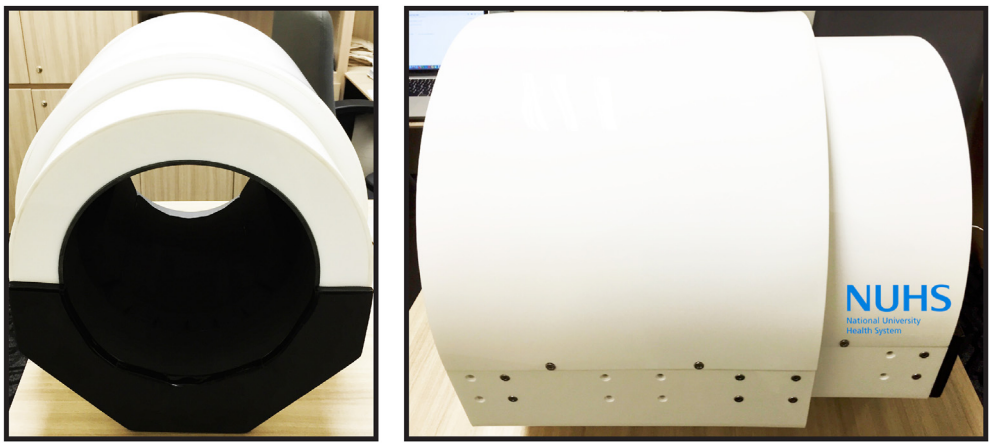

Fig. 1. PEMF prototype used in ACL-reconstructive surgery clinical trial at the National University of Singapore.

(hip-to-knee) by manual region drawing using the Medical Imaging Interaction Toolkit (MITK, version 2015.5.2). Regions delineated included subcutaneous fat, bone, vessels and tendons, and individual muscle groups: Adductor Magnus (AM), Biceps Long Head (BLH), Biceps Short Head (BSH), Gracilis (G), Rectus Femoris (RF), Sartorius (Sart), Semimembranosus (SM), Semitendinosus (ST), Vastus Intermedius (VI), Vastus Lateralis (VL), and the Vastus Medialis (VM).

2.6. Muscle lipid content

Muscle fat fraction data was acquired using a 2-point Dixon sequence with TE/TR = 9/600 ms, voxel size = 0.8 × 0.8 × 5mm^3, matrix = 256 × 256 × 32. Muscle regions of interest (ROIs) from volumetric images were resampled to the Dixon and were used to extract the individual muscle fat fractions (defined from the image signals (S) from the fat and water images: FF= $S_{fat}/(S_{fat} + S_{water})$).

2.7. Muscle macromolecular content

For assessment of Quantitative Magnetization Transfer (qMT) parameters, measurements were performed, as described by Sinclair et al. [32] using a gradient echo sequence with 350° and 500° MT pulse applied at the following frequencies; 1, 2, 5, 10, 20 kHz and two additional acquisitions with 500° MT pulse, at 50 and 100 kHz, assuming negligible MT at these frequencies. Acquisition parameters for qMT images were as follows: echo-time/repetition-time (TE/TR) = 3/50 ms, flip angle (FA) = 6°, field-of-view (FOV) = 200 × 200mm^2, 128 × 128 matrix, 16, 10 mm slices. A B_1-map was acquired using the Actual Flip Angle (AFI) Imaging sequence [33] and the following parameters: $TE/TR_1/TR_2$ = 3/50/150 ms, FA = 60°, 64 × 64 matrix, with FOV and slices matched to the qMT images. A T_1 map was acquired using DESPOT1 [34] with TE/TR = 3/25 ms, FA = 5,15 and 25°. FOV was matched to the qMT images.

B_1 maps were smoothed with a Gaussian kernel (extent = 4 voxels, sigma = 2) to reduce the effects of noise in the image propagating to T_1 maps. MTR images were corrected for B_1 inhomogeneity as described by Ref. [35] using a constant factor (k) across all subjects calculated from muscle-only regions in images. To extract the qMT parameters, all images were coregistered to the 100k, 500° MT image, using Advanced Normalization Tools (ANTs). Muscle masks (binary images defining the muscle-only region) were eroded (disk kernel, radius = 4 voxels) and downsampled to avoid edge/partial volume effects and to match the coregistered qMT images. The resulting median signals were fitted to a super-Lorentzian using a 2-parameter model for extraction of the qMT parameters and a trust-region-reflective algorithm in Matlab (version 2015a, Mathworks). Parameters for T_{2b}, the T_2 relaxation time for the bound pool, RM_0^A, the rate of exchange from the macromolecular to free pools, and $1/(R_A T_2^A)$, were all fixed to constants (6 μs, 12 s^{-1} and 50 respectively, R_A being the reciprocal of the longitudinal relaxation and T_2^A, the transverse relaxation of the free pool).

2.8. Lipidomics

Blood plasma samples were extracted using the methyl-tert-butyl ether with class-specific lipid internal standards and were analysed using a QExactive Plus mass spectrometer (Thermo Fisher Scientific, Bremen, Germany) and chip-based nanoelectrospray device (Advion Biosciences, Ithaca, NY, USA), with lipids detected in both polarities. Ceramides and acylcarnitines were separately analysed by reversed phase chromatography on an Agilent Eclipse Plus C18 reversed phase column in a Thermo Vanquish UHPLC system.

Direct infusion data were processed using LipidXplorer, while chromatographic data were processed using Lipid Data Analyzer. To ensure the quality of the results, samples were randomized and stratified prior to processing and analysis, bracketed and interspaced by replicate extractions of a pooled quality control sample, blank extracts and varying concentrations of a pooled sample to assess linearity. Only lipids that were detected reproducibly (coefficient of variation <20% in replicate samples), showed no signal in blank samples (<10% of pooled sample), and showed a linear behaviour were considered for further analysis.

2.9. Plasma biomarker analyses

Blood samples were obtained via venipuncture, and plasma was collected after centrifugation for 10 min at 1,000 x g at 4 °C. Quantitative determination of plasma Cathepsin B, BDNF, Osteopontin, Follistatin, Irisin, P3NP, and TNNT1 were evaluated by sandwich enzyme-linked immunosorbent assay and performed using R&D Systems Human Quantikine™ ELISA Kits (Bio-Techne, USA) and MyBioSource ELISA Kits (MyBioSource, USA). The absorbances were read using Tecan Spark multimode microplate reader platform (Tecan, Switzerland). Cathepsin B, BDNF, Osteopontin, Follistatin, Irisin, P3NP, and TNNT1 concentrations were determined using a standard curve (dynamic range of 0.156–10 ng/mL, 62.5–4000 pg/mL, 0.313–20 ng/mL, 250–16,000 pg/mL, 3.12–200 ng/mL, 3.12–100 ng/mL, and 3.12–1000 pg/mL, respectively) according to manufacturer's instructions (for details see Supplementary Table 3).

2.10. Targeted metabolomics for small molecule biomarkers

Targeted metabolomics of amino acids and oxidative stress-related small molecules was performed using Agilent 1290 Infinity II Liquid chromatography-6495C triple quadrupole tandem mass spectrometers (LC-MS/MS) in the multiple reaction monitoring (MRM) mode.

Chromatographic separations were achieved using a SeQuant®ZIC®-cHILIC HPLC column (Merck Pte Ltd, Singapore). All chromatograms for all metabolites were manually reviewed for signal quality and carryover. All analytes displayed linearity coefficient R2> 0.98. The acceptance criteria for the mean extraction recovery of all analytes was ≥85%. The acceptance criteria for the accuracy or relative error (RE) were all ≤15%, whereas the criteria for the precision obtained by calculating the within- and between-run coefficient of variation (CV) was ≤20%. For further details see Supplementary Table 4 and Supplementary Methods.

2.11. Statistical analysis

Results are presented as percentage changes from baseline (week 1 for MRI). pH data are presented as absolute change. MRI, plasma biomarker and ceramide data were assessed to be normally distributed using a Shapiro–Wilk test (excepting PME measures and P3NP), and as such are present as mean ± SD. Within-group data were analysed using a one-sample *t*-test, while between-group data were assessed using a Students *t*-test in SciPy. Ceramide data were analysed using paired two-sample *t*-tests. Metabolomic data tended to be non-normal and thus are presented as median (interquartile range) with within-group differences calculated using a one-sample Wilcoxon signed rank and between group differences assessed using a Mann–Whitney in SciPy. Dot plots and bar charts were generated using Graphpad Prism 9. All results were considered significant for $p < 0.05$ with no correction made for multiple comparisons.

3. Results

Baseline demographics for the two groups are shown in Supplementary Table 1.

3.1. ^{31}P MRS

Muscle bioenergetics and membrane kinetics were examined using ^{31}P MRS. Fig. 2a shows an example ^{31}P MR spectra obtained from one subject. No significant differences were detected between the PEMF-treated and control cohorts at week 1 post-ACLR.

PDE and PME are biomarkers for membrane breakdown and synthesis, respectively [36]. Elevations of PDE/ATP are found in obesity [37] and sarcopenia [38] and were observed in the control group (Fig. 2b; red), but not in the PEMF group (Fig. 2b; blue). This indicates significantly greater muscle breakdown in the control group.

Measures of PCr/ATP, Pi/ATP, Pi/PCr, (Pi + PCr)/ATP and pH reflect the bioenergetic status of muscle. An increase in the P_i/PCr ratio characterizes muscular mitochondrial dysfunction and metabolic stress [39,40] and was observed in the control cohort (Fig. 2c; red, right). An increase in (Pi + PCr)/ATP was also observed in the control cohort (Fig. 2c; red), indicative of decreases in ATP, as previously reported for diabetics [41]. The control cohort also exhibited larger increases in PCr/ATP and Pi/ATP, consistent with muscle mitochondrial dysfunction following surgical immobilization. Notably, PEMF treatment ameliorated the increments in Pi/PCr, Pi/ATP and PCr/ATP observed in the control cohort, suggesting metabolic stabilization.

Muscle acidification was also attenuated in the PEMF cohort (Fig. 2c; blue, bottom) which may indicate reduced reliance on anaerobic ATP production. Accordingly, the employed magnetic exposure paradigm has been shown to activate PGC-1α transcriptional pathways [29], associated with the attenuation of muscle lactate production to enhance exercise performance and metabolic health [42]. Also see Supplementary Table 5 for precise significance values.

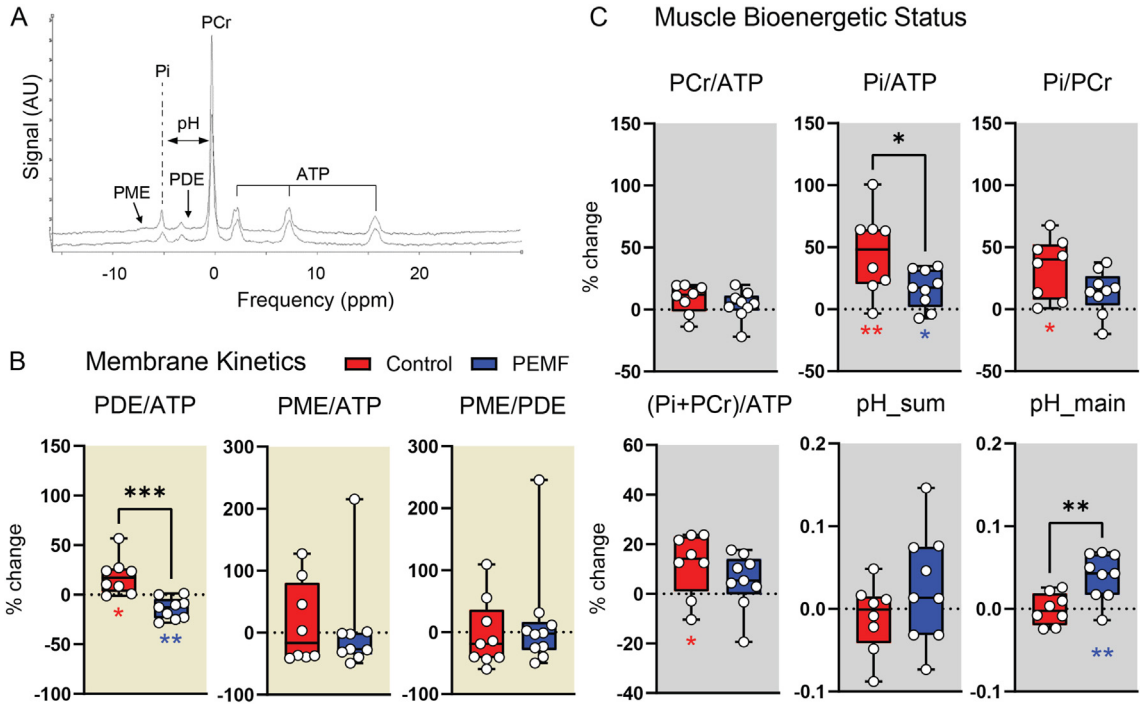

Fig. 2. ^{31}P MRS analysis of the operated limbs of ACLR patients following 16 weeks of PEMF therapy (blue) or sham intervention (red). (A) Representative spectra showing the signal intensities and frequencies (ppm) of the various ^{31}P metabolites. (B) and (C) show the dot-plots of the changes in ^{31}P metabolite ratios for the assessment of membrane turnover kinetics (PDE/ATP, PME/ATP and PME/ATP) (B) and bioenergetics status (PCr/ATP, P_i/ATP, P_i/PCr, (Pi + PCr)/ATP and pH) (C) as indicated. pH was calculated from the mean weighted shift of the P_i to PCr peak using equation derived by Ref. [72]. Several patients' ^{31}P MRS data was excluded in the analysis due to an unknown reduction in signal-to-noise ratio (SNR) (~1/4 of other scans). Statistical significance is shown as $^{*}p < 0.05$, $^{**}p < 0.01$ and $^{***}p < 0.001$ based on one-sample *t*-test and two sample unpaired *t*-test for within-group and between-group tests respectively. N = 8 for sham intervention and N = 9 for PEMF intervention. The error bars show the min and max of the % change. Also see Supplemental Table 5.

3.2. Plasma biomarker analysis

Changes in the levels of plasma biomarkers indicative of muscle homeostasis were examined post-ACLR. Osteopontin, associated with states of active muscle regeneration [43,44], was significantly elevated in the PEMF-treated cohort, but not in controls (Fig. 3a-b). Elevated levels of TNNT1 (Troponin T1, Slow Skeletal Type) characterize states of physical inactivity and oxidative (slow) muscle loss [45]. TNNT1 plasma levels were significantly reduced in the PEMF-treated cohort relative to the control cohort (Fig. 3c-d), agreeing with a reported propensity of PEMF exposure to promote oxidative muscle development [29,30]. Follistatin sustains muscle development by inhibiting the actions of myostatin and showed a non-significant trend to increase in the PEMF cohort (Fig. 3e-f). Irisin levels were significantly elevated in the control cohort, but not PEMF cohort (Supplemental Table 6). Irisin, despite being commonly described as an exercise-induced myokine [4], is secreted from white

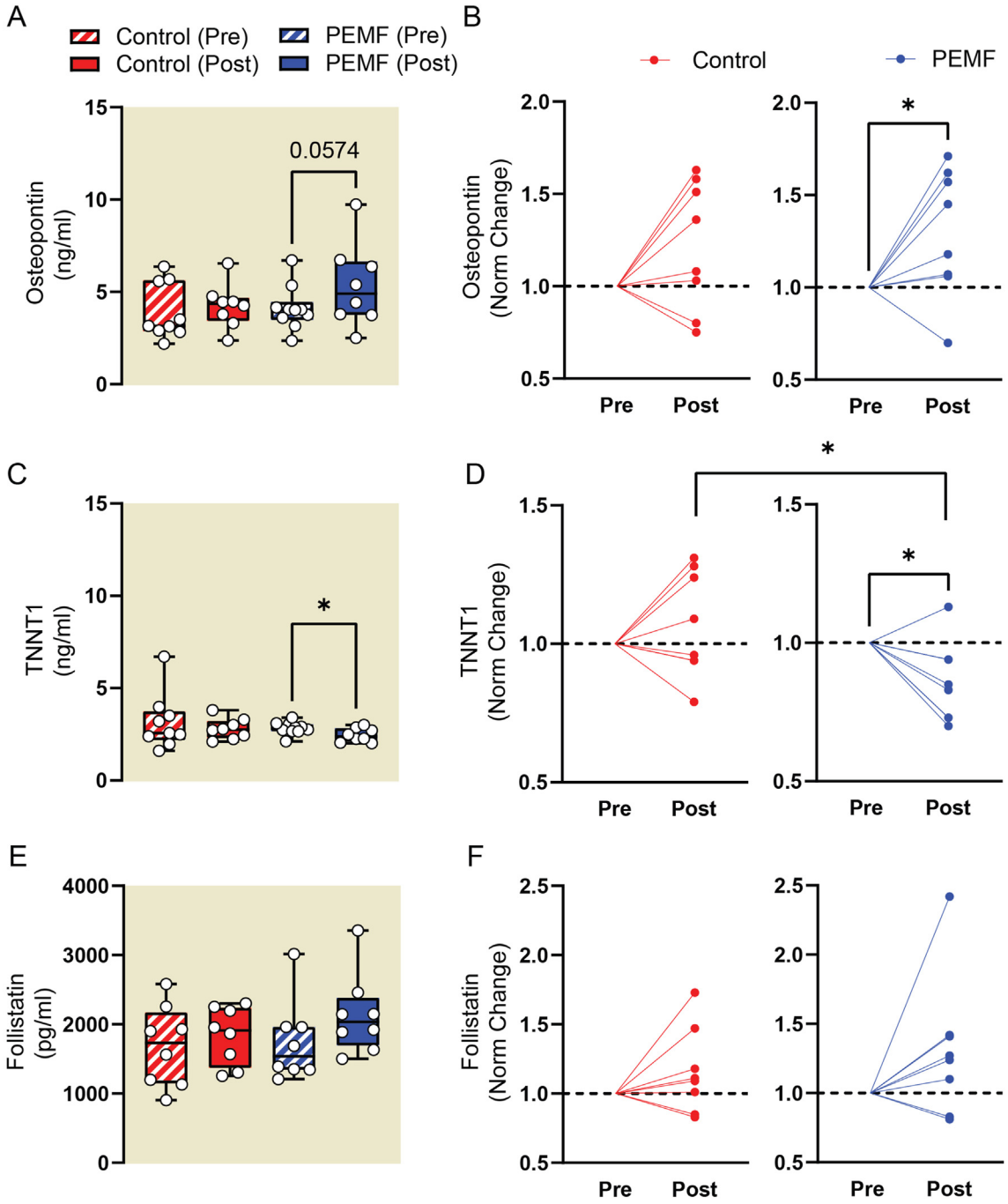

Fig. 3. Plasma biomarker analysis measured using ELISA. The absolute concentration (left) and normalized values showing change from starting concentration values (right) for plasma Osteopontin in (A) and (B), plasma TNNT1 in (C) and (D), and for plasma Follistatin in (E) and (F). The statistical analyses for (A), (C) and (E) were done using One-Way ANOVA (Mixed-effect analysis) with Sidak's multiple comparisons test. The error bars show the min and max of the absolute concentrations. The statistical analysis for (B), (D) and (F) was performed using two-sample unpaired *t*-test, with $*p < 0.05$ for all analyses. Red labels represent the sham control cohort while blue labels represent cohort with magnetic intervention. N = 8–9 for control group and N = 9–10 for PEMF group. Some samples were excluded from analysis due to substantial hemolysis during blood collection. Also see Supplementary Table 6 for the tabulation of *p* values of the present data and other analytes.

adipose tissue in obese animals and humans as well as is positively correlated with body fat mass [46]. Irisin levels are also high in those with insulin resistance and metabolic syndrome [47].

3.3. Plasma metabolomics

Meta-analysis has shown that elevated levels of arginine, phenylalanine, tyrosine and isoleucine are associated with higher diabetes risk [48]. Plasma arginine (Fig. 4a), phenylalanine (Fig. 4b) and tyrosine (Fig. 4c) were elevated in the sham control cohort (red) relative to the PEMF cohort (blue) at 16 weeks after ACLR, whereas differences in isoleucine levels did not reach statistical significance (Fig. 4d). Elevated homocysteine and cysteine levels are positive predictors of mitochondrial dysfunction and metabolic disturbances, and are linked to methionine metabolism [49,50]. Plasma homocysteine levels were reduced in the PEMF cohort (Fig. 4e; blue), whereas plasma cysteine levels were elevated in the sham control cohort 16 weeks after ACLR (Fig. 4f; red). Similarly, plasma methionine levels were significantly elevated in the sham group (Fig. 4g; red). Moreover, changes in plasma cysteine (Fig. 4f) and methionine (Fig. 4g) were significantly different between cohorts at study termination, exhibiting lower levels in the PEMF cohort. Histidine is an amino acid with anti-oxidant and pH buffering capabilities [51]. Histidine is converted into carnosine (requiring mitochondrial ATP hydrolysis) and buffers changes in intramyocellular pH during anaerobic glycolysis and is associated with metabolic stability. Histidine levels were elevated in the control cohort (Fig. 4h) and may be related to the detected acidosis herein (Fig. 2c (pH) and Supplemental Table 5). Disrupted histidine catabolism correlates with elevated methionine and homocysteine levels [52] and would mirror thus mirror the changes detected in the control cohort. The changes for other small molecule biomarkers are given in Supplemental Table 7.

3.4. Plasma lipidomics

Changes in plasma ceramide (Fig. 5a–b) and lysophosphatidylcholine (Fig. 5c) levels were compared between PEMF- (Fig. 5; blue) and sham-treated (Fig. 5; red) cohorts. While plasma ceramide levels were indistinguishable between cohorts at the start of the study (Fig. 5a; hatched), they were significantly reduced at study termination in the PEMF-treated cohort (Fig. 5a; solid). Moreover, whereas plasma ceramide levels tended to rise in the control cohort during the study period, they dropped in the PEMF-treated cohort (Fig. 5b). Certain lysophosphatidylcholine species levels were also significantly reduced following magnetic therapy relative to the control cohort (Fig. 5c).

3.5. Muscle MR dixon and volumetric measures

No significant differences in muscle cross-sectional areas or fat measures were found between cohorts at study commencement (week 1). Percentage changes in muscle volumes and fat fractions at week 16, compared to week 1, are shown in Fig. 6a and b, respectively. Expectedly, the gracilis and semitendinosus (graft donor muscles) exhibited significant reductions in muscle volumes and large increases in fat content. Contrastingly, the other muscles tended to show increases in volume that were of similar magnitude between groups. Subcutaneous fat levels were significantly increased in both groups to similar degrees. Intramuscular fat content tended to be greater in the PEMF cohort, but was not significantly different across groups. Although muscular fat arising during metabolic disruption is predictive of muscle loss of function [53], high levels of muscle lipid are also seen in highly trained endurance athletes, compared with untrained controls, likely due to differences in cellular metabolic adaptation or fibre type composition [25]. Individual fat and muscle values are provided in Supplemental Table 8.

3.6. qMTR parameters

Fig. 7a shows example B_1 and T_1 maps and extracted MTR images from one patient at weeks 1 and 16 post-ACLR. Fig. 7b gives the composite MTR parameters for the entire upper leg musculature and Fig. 7c–g depicts the same parameters for the individual muscles: T_{1obs}, the measured longitudinal relation time; MTR, calculated from the 1000Hz, 350° MT_{on} image and the 100 kHz 500° image (MT_{off}, assuming this has negligible MT) using $MTR = 100*(MT_{off}\text{-}MT_{on})/MT_{off}$; T_1^A and $T2^A$, the longitudinal and transverse relation times for the free pool; F, the fraction of protons in the bound pool relative to those in the free pool; and R/g, the rate of exchange of bound to free protons (R), scaled by a scanner specific parameter (g).

The PEMF group showed overall greater increases in MTR measures. Increases in the longitudinal relaxation constant (T_{1obs}) and the relaxation constant of the free pool (T_{2a}) were only seen in the PEMF group. Comparison of the parameters indicates similar changes between analogous muscles, with a tendency for larger changes in the donor muscles (gracilis and semitendinosus). In general, increases in MTR, T_{1obs}, T_{2A} and F were observed, accompanied by decreases in R/g. Results were similar for both groups with a tendency for larger changes in the PEMF cohort. Specific MTR values are provided in Supplemental Table 9.

4. Discussion

Preclinical studies conducted with this same magnetic platform have shown that PEMF exposure activates PGC-1α-dependent transcriptional cascades promoting *in vitro* [29] and *in vivo* [30] myogeneses and downstream of mitochondrial adaptive responses. Consistent with PGC-1α involvement, PEMF exposure demonstrated a predilection to enhance oxidative muscle expression in cells [29] and mice [30]. The murine study also demonstrated PEMF-induced enhancements of adipose browning, fatty acid oxidation and insulin-sensitivity [30] that would be consistent with the reductions in plasma ceramide levels demonstrated in the present study. Elevated ceramides are associated with systemic lipotoxicity, inhibition of adipose browning and insulin-resistance [20,21]. To what extent the human condition will parallel the mouse phenotype remains to be shown.

4.1. Evidence for muscle mitochondrial dysfunction following ACLR

^{31}P MRS analysis showed increases in P_i/ATP, PCr/ATP, (P_i + PCr)/ATP and P_i/PCr in both cohorts, although generally greater in the control cohort (Fig. 2c). Increases in P_i/PCr are generally seen upon increased metabolic demand, such as during exercise, when ATP utilization cannot be met by oxidative phosphorylation and must be regenerated via direct phosphorylation from PCr. Elevations in P_i/PCr may thus either indicate increased ATP demand or decreased ATP production due to mitochondrial dysfunction. Increases in P_i are also generally mirrored by decreases in PCr. Thus, larger (Pi + PCr)/ATP ratios, as seen in the control cohort, corroborate a reduction in mitochondrial ATP production. The magnitude of the increments in P_i/PCr and (P_i + PCr)/ATP were significantly smaller in the PEMF group (Fig. 2c), indicating an amelioration of muscular bioenergetic dysfunction post-ACLR.

Additionally to changes in ^{31}P MRS, plasma homocysteine and cysteine levels, markers of mitochondrial dysfunction and linked to methionine metabolism, were elevated in the sham group relative to PEMF therapy at week 16 post-ACLR, indicative of metabolic improvement (Fig. 4).

4.2. Changes in blood ceramide levels following ACLR and PEMF therapy

Physical inactivity and obesity result in the accumulation of cytotoxic palmitate-derived ceramides that are associated with attenuated muscle growth and metabolic dysfunction [20]. Accordingly, reductions in

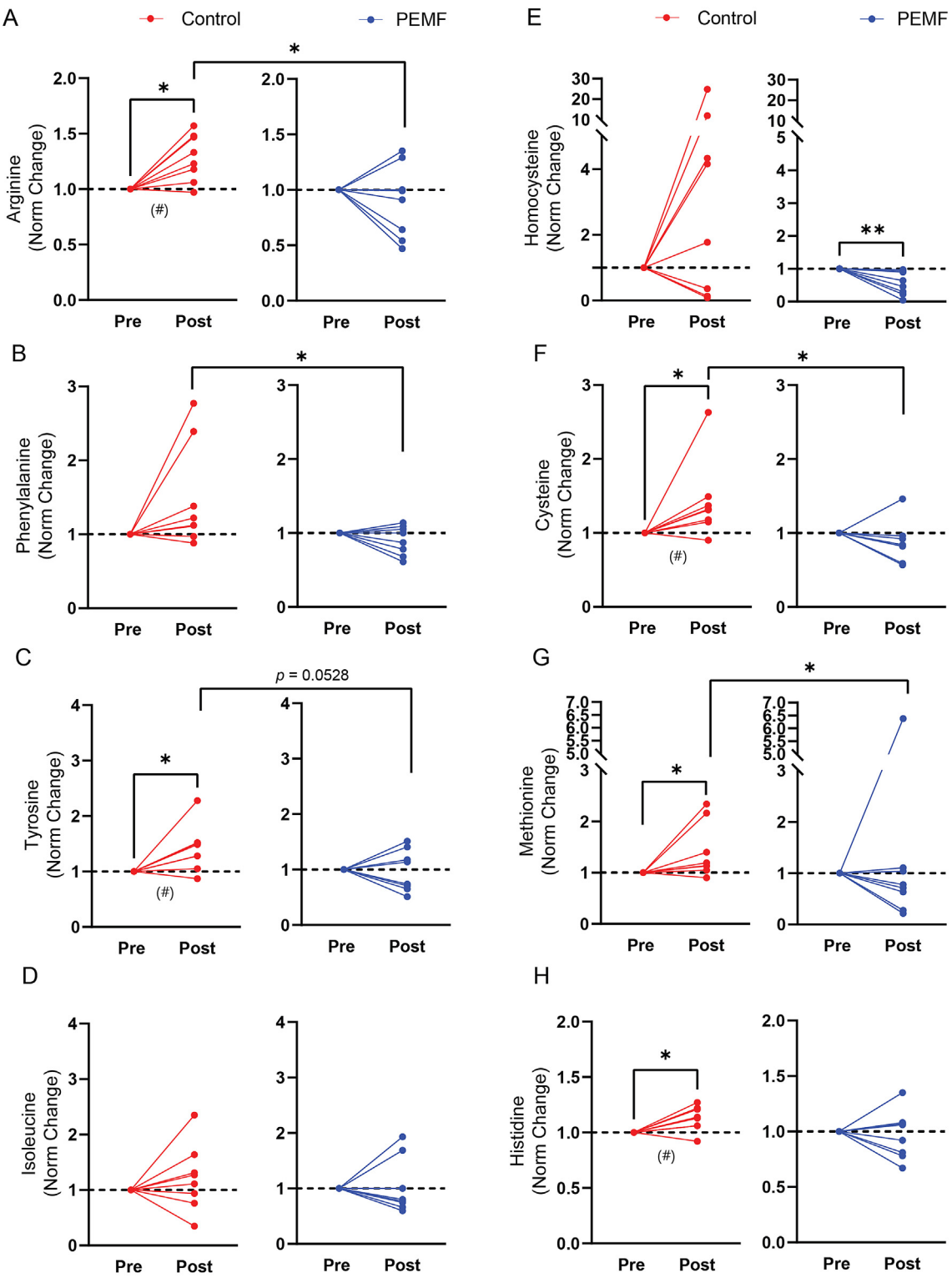

Fig. 4. Targeted metabolomics for small molecule biomarkers of oxidative stress and metabolic disruption detected using LC-MS-MS. Plasma levels of arginine (A), phenylalanine (B), tyrosine (C), isoleucine (D), homocysteine (E), cysteine (F), methionine (G) and histidine (H) 16 weeks after ACLR were normalised to their respective preoperative levels for each subject. No significant differences were found between groups at the onset of the study. Blue lines represent those subjects receiving magnetic intervention; red represents the sham control cohort. Also see Supplemental Table 7. Statistical analysis for within-group was carried out using a one-sample Wilcoxon and between-groups using a Mann–Whitney U, with $*p < 0.05$ and $**p < 0.01$. N = 8–9 for control group and N = 9–10 for PEMF group. $^{\#}p < 0.05$ represents the statistical significance also presented in Supplemental Table 7.

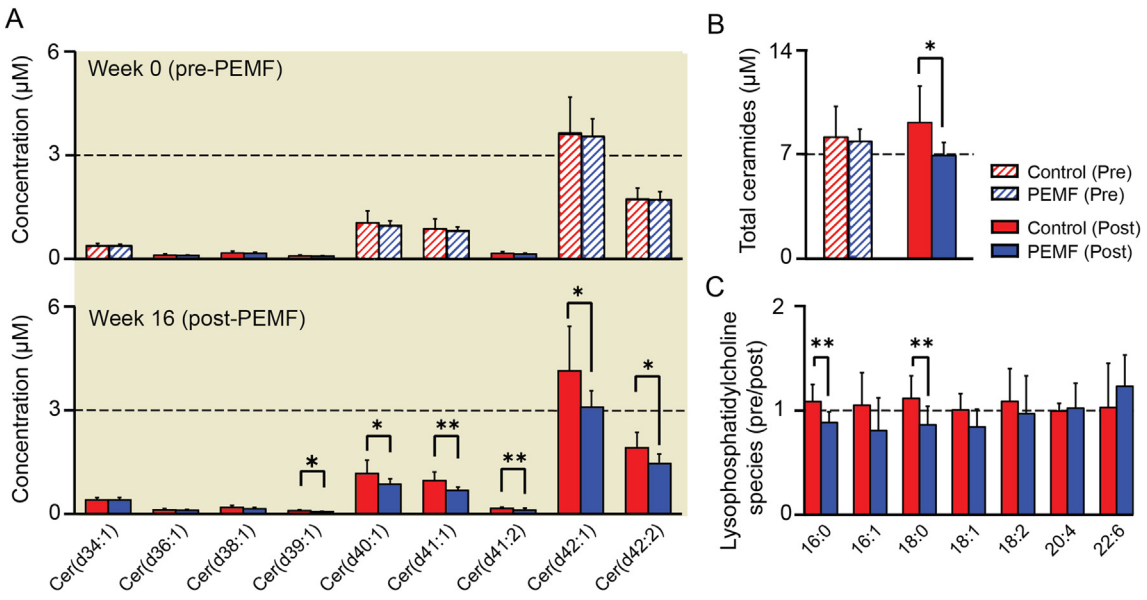

Fig. 5. Plasma ceramides levels. (A) Shows the concentration of ceramide species at week 0 (upper panel) and at week 16 (lower panel), and (B) shows the total ceramides concentration. Plasma ceramide levels were indistinguishable between PEMF-treated (Blue) and control (Red) cohorts at study commencement (week 0). The bar charts in (C) shows the normalized values of specific lysophosphatidylcholine species before and after 16 weeks from the date of ACLR. Blue bars represent those subjects receiving magnetic intervention; Red bars represent the sham control cohort. The data were analysed using two-sample paired *t*-test, with $*p < 0.05$ and $**p < 0.01$ and the error bars represent the standard error of the mean. N = 8 for control group and N = 9 for PEMF group.

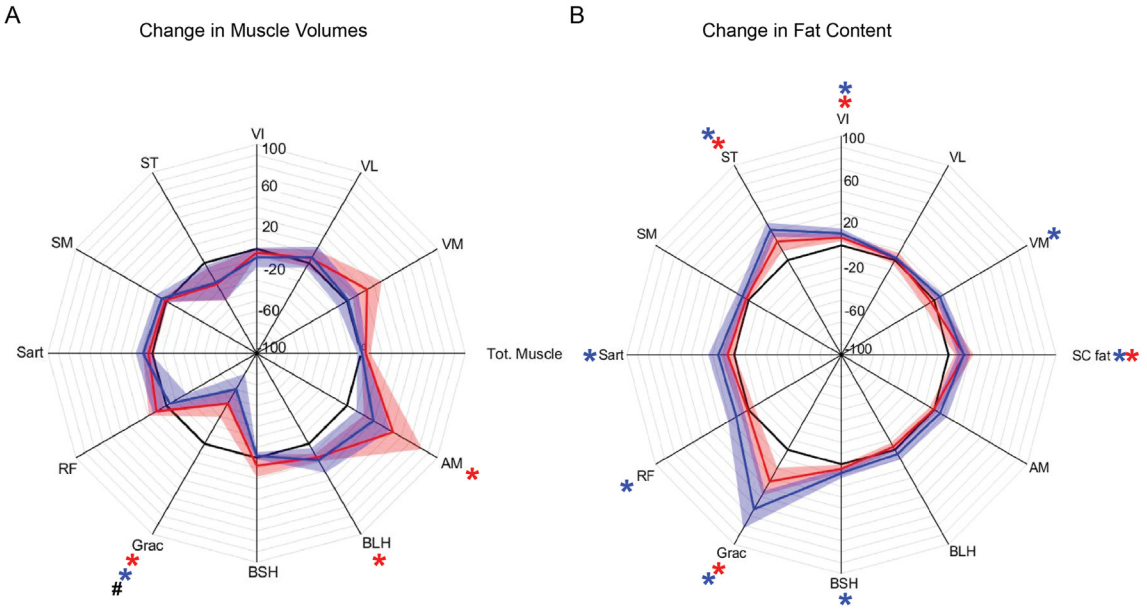

Fig. 6. Muscle Volume and Fat Content. (A) Shows the change in the total thigh muscle volume as well as the breakdown of the individual thigh muscles. (B) Shows changes in the fat distribution in the thigh including the subcutaneous fat and individual muscle fat content. Blue regions represent those subjects receiving magnetic intervention; red represents the sham control cohort. Data are percentage median ± interquartile range relative to baseline (black line denotes 100% of baseline value). Significant within-group differences are indicated by *, and between-group differences are denoted by # all at $p < 0.05$, with N = 8 for control group and N = 9 for PEMF group. Also see Supplemental Table 8 for measured changes in muscle volumes and fat fractions.

skeletal muscle ceramide levels are associated with improved systemic insulin sensitivity [18], whereas elevated blood ceramide levels are instead characteristic of states of physical immobilization, sedentary lifestyles [17,19] and metabolic disruption [17]. Longer ceramide species have also been shown to be toxic to mitochondrial function [20,54]. The lysophosphatidylcholines are another class of palmitate-derived lipid metabolites of potential toxicity [22]. Elevations of lysophosphatidylcholine levels characterize sarcopenic muscle, wherein preventing lysophosphatidylcholine synthesis reinstates a youthful lipid profile, reduces metabolic stress, improves protein synthesis and promotes muscle recovery [23]. We observed significant reductions in certain plasma ceramide and lysophosphatidylcholine species in the PEMF therapy group relative to the sham control cohort (Fig. 5).

4.3. *Muscle degeneration following ACL surgery and PEMF therapy*

PMEs and PDEs have been implicated in cellular membrane turnover [36]. Increases in the PDE/ATP ratio reflect increased membrane

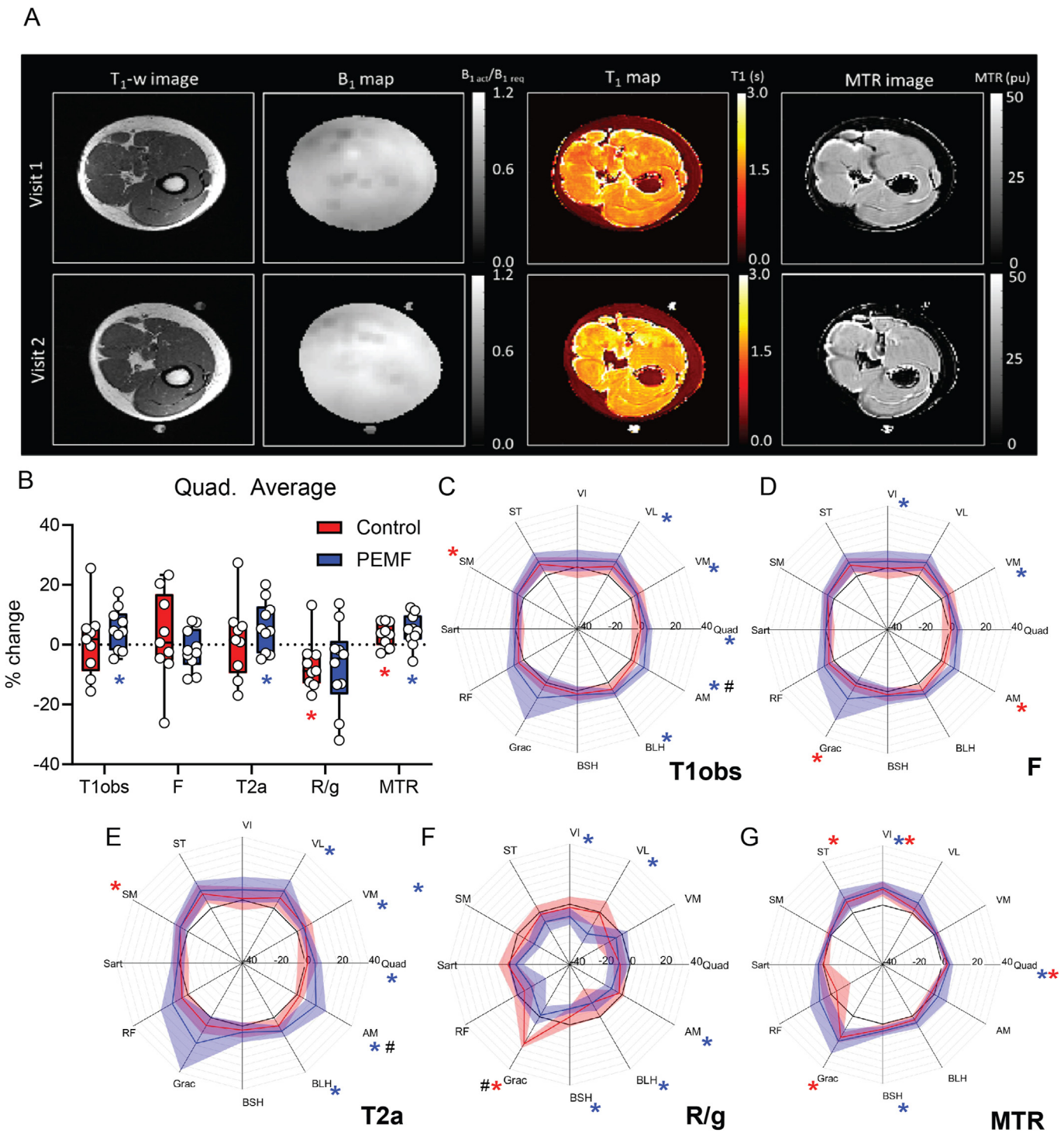

Fig. 7. Quantitative Magnetic Transfer (A) Shows example qMT images from a single subject including at (top) week 1 and (bottom) week 16. These include (left to right) T_1-weighted anatomical image, B_1 map, T_1 map and MTR image. Images were fit to a 2-parameter model providing parameters $T1_{obs}$, F, $T2_A$, $T1_A$, R/g and MTR (B) Shows the % change from baseline in the quadriceps. Data presented are percentage change from week 1, (C)-(G) are the percent of baseline values for the individual muscles with 100% denoted by the black line. Within-group changes represented by *, and between-group differences represented by # at $p < 0.05$. One subject's quantitative magnetization transfer (qMT) data was removed due to significant motion during visit 1 (Control group) which lead to poor fitting of qMT data (assessed from the chi-squared value). Blue regions represent those subjects receiving magnetic intervention, N = 9; red represents the sham control cohort, N = 8. Also see Supplemetal Table 9 for measured changes in MTR values from the Quads.

breakdown. The increases in PDE/ATP observed in control patients were reversed in the PEMF cohort, suggesting an amelioration of membrane breakdown and is in agreement with the relatively elevated levels of osteopontin in the PEMF group. Increases in muscle PDE/ATP are also correlated with extensive fat infiltration in Duchenne muscular dystrophy [55].

4.4. Changes in whole muscle qMT parameters following ACLR and PEMF therapy

MTR measures drop following injury [56] and are negatively correlated with muscular fat fraction [57]. Our results hence suggest that muscle recovery at 16 weeks was greater in the PEMF group, wherein MTR measures generally increased. By contrast, increases in T_2, as seen here in the PEMF cohort, occur early in tissue injury/disease due to edema, prior to lipid infiltration [58]. Increases in T_2 are also seen in myopathies [59] and predict inflammation [60]. Therefore, based on this parameter, the PEMF group may present greater levels of inflammation/edema/fat. On the other hand, inflammation-correlated changes in F [56], are opposite to those observed in the PEMF cohort. In summary, increases in MTR suggest muscle improvements, particularly in the PEMF group, yet is confounded by some indications of greater inflammation in the PEMF cohort.

Exercise-induced increases in T_1 and T_2 [61], were recapitulated in the PEMF group, but on a smaller scale. Increases in T_1 and T_2 may signify changes in muscle perfusion in response to metabolic demand and in the context of PEMF treatment may either reflect edema or possibly enhanced metabolic status, which would coincide with the ^{31}P MRS data (Fig. 2). The fact that changes in MTR, T_{1obs} T_{1a} and T_{2a} as well as R/g tended to be larger in the PEMF cohort, however, corroborate our other indications of accelerated muscle recovery. More work is needed to fully understand the cellular mechanisms behind the observed changes in qMT parameters.

4.5. Study limitations and insights

4.5.1. Study powering

Despite the small cohort sizes, we detected significant changes in local muscle bioenergetics and indices of systemic lipotoxicity [22] between cohorts. Not only were these changes significant at an individual level, but the directions of the changes across measures were consistent with expected physiological changes, which is a much stronger indication that the null hypothesis should be thrown out. Statistically, since these are largely independent metabolic measures, their individual powers can be multiplied.

4.5.2. Fiber Type–Fiber size paradox

Despite noted metabolic improvements, weekly PEMF treatment nominally changed muscle volume (Fig. 6a), more generally increased muscle adipose content (Fig. 6b) and did not significantly change muscle force generation (Supplementary Fig. 1). These features align with the propensity of our magnetic field paradigm to promote oxidative muscle development in cells [29] and animals [30] via the PGC-1α transcriptional pathway, upstream of mitochondriogenesis. First, in response to aerobic training, an inverse relationship exists between muscle oxidative capacity and muscle size as a consequence of the prioritizing of mitochondrial over myofibrillar biosyntheses, governing muscle metabolic and contractile adaptations, respectively, that ultimately sacrifices muscle power (and mass) for resistance to fatigue [62]. Specifically, heightened mitochondrial biogenesis, downstream of AMP-activated protein kinase and PGC-1α transcriptional cascades, result in an overall attenuation of muscle protein anabolism. An inverse relationship has been also shown to exist between striated muscle fibre cross-sectional area and oxidative capacity [62], whereby higher VO_{2max} correlated with smaller calibre fibres. Accordingly, we have previously shown that oxidative fibre cross-sectional area was reduced by weekly PEMF treatment in mice, yet was associated with enhanced running performance and stimulated respiratory exchange ratio, associated with the elevated respiratory combustion of fats [30]. In essence, a reduction in fibre cross-sectional area increases surface to volume ratio, facilitating oxygen uptake into oxidative fibres with heightened mitochondrial respiration, and PGC-1α activity [62]. Secondly, the high caloric value of lipids makes them the preferential energy source for sustained muscular activity [24]. Therefore, mitochondrial activation and downstream recruitment of PGC-1α transcriptional cascades, whether by muscle contraction [24] or PEMF exposure [30], increases muscular mitochondrial fatty acid oxidation. Accordingly, intramyocellular lipid content also increases with training and is highest in oxidative muscle [25]. Muscle is thus capable of preferentially storing lipids when energy demand is high, as during training, or sequester lipids as a default when plasma-free fatty acids are abundant, as during obesity or high dietary fat intake. Thirdly, as enhancements in muscular oxidative capacity occur at a compromise to muscle power and mass [62], measuring power output, rather than endurance capacity, was less directly applicable to the physiological adaptations instilled by our magnetic intervention. Finally, oxidative muscle fibers in the leg musculature are preferentially lost in response to disuse following ACLR [63], addressing the relevancy of our proposed therapeutic strategy. Activation of the PGC-1α pathway by PEMF exposure is therefore consistent with our presented human results and of fundamental clinical importance.

4.5.3. Magnetically-induced oxidative stress

The employed magnetic paradigm produces a low level of oxidative stress that, while adaptive in nature in healthy tissues [29,64], may reach damaging levels in metabolically inflamed tissues [65]. Therefore, the exposure of an operated limb with aggravated and surgically-inflamed lesions may not have been the best therapeutic approach. The observation that the lesioned muscles donating the surgical graft, the gracilis and semitendinosus, underwent the greatest degree of muscle atrophy (Fig. 6a) and lipid accumulation (Fig. 6b) in the operated limbs receiving magnetic exposure (blue) aligns with this precaution, as do our qMTR measurements suggesting greatest levels of inflammation in these same graft donor muscles (Fig. 7). In support of potential localized PEMF-induced inflammation, we have recently shown that direct exposure of muscle cells to analogous PEMFs resulted in the induction of oxidative stress that, whilst required to elicit a secretome response for subsequent myogenic enhancement, incurred a small degree of local developmental depression [64]. By contrast, the provision of PEMF-induced secretome to naïve muscle cells resulted in greater developmental enhancement, without eliciting oxidative stress. The PEMF-induced secretome of MSCs has also been previously shown to confer protection against induced inflammation [66]. In this regard, the systemic effects observed in the present study may thus have arisen from the muscle secretome [4,5] released in response to magnetic field exposure [66,64]. That is, the magnetically-stimulated leg musculature likely provided systemic secretome "feeding" with anti-inflammatory agents that may have underlined our observed metabolic improvements. Somewhat unexpectedly therefore, exposure of the unoperated leg may have served as a better rehabilitation scenario for averting inflammation of the operated leg as well as for inducing muscle secretome release from a healthy limb for overall systemic benefit.

4.5.4. Contralateral or cross-education effects

A contralateral effect has been described, whereby exercising one limb prevents the atrophy of an immobilized contralateral limb [67,68]. Such studies have generally shown that eccentric exercise of the dominant arm [69], or leg [70], protects against the loss of size and function of the contralateral limb. Although investigators have commonly invoked neurological origins to explain the cross-educational response, to the best of our knowledge, mechanistic evidence in support of this have not been directly provided. It has been demonstrated that unilateral immobilization of a limb results in systemic metabolic disruption characterized by mitochondrial dysfunction in the immobilized limb [71], aligning with the results of the present study. Indeed, the clinical potential and implications of contralateral rehabilitation have not gone unnoticed [68].

According with a contralateral effect, measurements of upper leg cross-sectional areas (CSA) indicated that muscle atrophy reverted sooner in the contralateral limbs of ACLR patients having received PEMF therapy (Supplementary Figs. 1a and b). Notably, CSA measurements of

the operated limb would suggest that MRI assessment (at week 16) was made at a time when muscle atrophy had already largely recuperated. Measurements of muscle force generation also showed a trend to improve more in the contralateral side of the PEMF cohort (Supplementary Figs. 1c and d; Q1 and Q2), despite failing to reach statistical significance. Our future studies will encompass a more thorough analysis of the magnetically-induced blood-borne factors and their contribution to the contralateral limb effect for improved therapeutic efficacy and ultimate clinical exploitation.

5. Conclusions

Metabolic biomarkers were the most significantly altered by our magnetic intervention. To our knowledge, this is the first study to show magnetically-induced changes in muscle bioenergetics status and membrane kinetics in humans following ACL reconstruction surgery. Notably, the energetic dysfunction observed immediately following ACL reconstruction (changes in P_i/PCr and P_i/ATP) could be significantly corrected by brief weekly PEMF treatment. In addition, suspected indices of systemic lipotoxicity could be reverted with magnetic field therapy. Magnetic field therapy may hence represent a potential treatment modality for improving muscle metabolic function following immobilizing surgery and does not interfere with positive rehabilitative physical outcome, offering a broadened therapeutic value by combining physical and magnetic therapies. These metabolic changes are sufficiently provocative to merit subsequent follow-up in larger clinical trials examining the effects of brief (10 min) weekly PEMF exposure on systemic metabolic homeostasis.

Author contributions

Mary C. Stephenson was involved in data acquisition, analysis and interpretation of the MRI data as well as the writing of the manuscript. Craig J.K. Wong was involved in the analysis and interpretation of the MRI. Y.K. Tai was involved in the interpretation and preparation of the manuscript. Jocelyn Naixin Yin and Rina Malathi Pannir Selvan helped in data gathering, plasma protein analysis, managing IRB submissions and running the study according to GCP and local regulations. Jürg Fröhlich and Christian Beyer conceptualized and designed the PEMF device while Jing Ze Li managed the fabrication of the PEMF device. Federico Torta, Alexander Triebl and Markus Wenk conducted the lipidomic and associated data analyses. Leroy S. Pakkiri and Chester Drum conducted the LS/MS MS and its analyses. Chun-Kit Wong and Shi-Jie Toh were involved in data analysis and John J. Totman was involved in data collection. Lingaraj Krishna and Alfredo Franco-Obregón designed the study. Lingaraj Krishna, Sara S. Tan and Duraimurugan Chinnasamy provided clinical assessment and/or conducted the surgical work. Alfredo Franco-Obregón secured the funding for the fabrication of the PEMF device and running of the study as well as contributed to the analysis and interpretation of the data as well as writing of the manuscript. All authors listed have read and approved this manuscript.

Funding support

This work was supported by the NUHS-CG CIRC Seed Funding Singapore (CIRC/P/2014/010), Singapore-MIT Alliance for Research and Technology Centre (SMART) ING14085-BIO (ING) and the Lee Kong Chian Medtech Initiative Fund (E−551-00-0607-01).

Declaration of competing interest

AFO, JF and CB are inventors on patent WO 2019/17863 A1, System, and Method for Applying Pulsed Electromagnetic Fields, AFO and JF are contributors to QuantumTx Pte. Ltd., which elaborates electromagnetic field devices for human use. JZL is currently an employee of QuantumTx Pte. Ltd, but at the time of writing the manuscript was an employee of the NUS, Department of Surgery. All other authors declare that they have no known competing financial interests or personal relationships that could have appeared to influence the work reported in this paper.

Acknowledgments

We are grateful to the Medical Engineering Research & Commercialization Initiative (MERCI) of the Department of Surgery, Yong Loo Lin School of Medicine of the National University of Singapore (NUS) for outsourcing the fabrication of the PEMF prototype used in this study. The authors would like to acknowledge Zac Goh (iHealthtech, National University of Singapore) for the production of the graphical abstract. This study was funded by the National University Health System Internal Grants (Clinical Imaging and Research Center Seed Funding), The Singapore-MIT Alliance for Research and Technology (SMART) Innovation Center Ignition fund and the Lee Foundation, Singapore. Additional thanks to radiographers, Tiang-Siew Yap and Serena Teo, for assistance with image acquisition and analysis.

Appendix A. Supplementary data

Supplementary data to this article can be found online at https://doi.org/10.1016/j.jot.2022.09.011.

References

[1] Fealy CE, Grevendonk L, Hoeks J, Hesselink MK. Skeletal muscle mitochondrial network dynamics in metabolic disorders and aging. Trends Mol Med 2021;27(11):1033–44. https://doi.org/10.1016/j.molmed.2021.07.013.
[2] Appell H-J. Muscular atrophy following immobilisation. Sports Med 1990;10(1):42–58. https://doi.org/10.2165/00007256-199010010-00005.
[3] Trevino MB, Zhang X, Standley RA, Wang M, Han X, Reis FC, et al. Loss of mitochondrial energetics is associated with poor recovery of muscle function but not mass following disuse atrophy. Am J Physiol Endocrinol Metab 2019;317(5):E899–910. https://doi.org/10.1152/ajpendo.00161.2019.
[4] Louzada RA, Bouviere J, Matta LP, Werneck-de-Castro JP, Dupuy C, Carvalho DP, et al. Redox signaling in widespread health benefits of exercise. Antioxidants Redox Signal 2020;33(11):745–60. https://doi.org/10.1089/ars.2019.7949.
[5] Scheele C, Nielsen S, Pedersen BK. ROS and myokines promote muscle adaptation to exercise. Trends Endocrinol Metabol 2009;20(3):95–9. https://doi.org/10.1016/j.tem.2008.12.002.
[6] Barker T, Henriksen VT, Rogers VE, Trawick RH. Improvement in muscle strength after an anterior cruciate ligament injury corresponds with a decrease in serum cytokines. Cytokine 2015;73(1):199–202. https://doi.org/10.1016/j.cyto.2015.01.036.
[7] Mendias CL, Lynch EB, Davis ME, Sibilsky Enselman ER, Harning JA, DeWolf PD, et al. Changes in circulating biomarkers of muscle atrophy, inflammation, and cartilage turnover in patients undergoing anterior cruciate ligament reconstruction and rehabilitation. Am J Sports Med 2013;41(8):1819–26. https://doi.org/10.1177/0363546513490651.
[8] Konishi Y, Oda T, Tsukazaki S, Kinugasa R, Fukubayashi T. Relationship between quadriceps femoris muscle volume and muscle torque at least 18 months after anterior cruciate ligament reconstruction. Scand J Med Sci Sports 2012;22(6):791–6. https://doi.org/10.1111/j.1600-0838.2011.01332.
[9] Konishi Y, Ikeda K, Nishino A, Sunaga M, Aihara Y, Fukubayashi T. Relationship between quadriceps femoris muscle volume and muscle torque after anterior cruciate ligament repair. Scand J Med Sci Sports 2007;17(6):656–61. https://doi.org/10.1111/j.1600-0838.2006.00619.
[10] Lindström M, Strandberg S, Wredmark T, Felländer-Tsai L, Henriksson M. Functional and muscle morphometric effects of ACL reconstruction. A prospective CT study with 1 year follow-up. Scand J Med Sci Sports 2013;23(4):431–42. https://doi.org/10.1111/j.1600-0838.2011.01417.
[11] Paterno MV, Schmitt LC, Ford KR, Rauh MJ, Myer GD, Huang B, et al. Biomechanical measures during landing and postural stability predict second anterior cruciate ligament injury after anterior cruciate ligament reconstruction and return to sport. Am J Sports Med 2010;38(10):1968–78. https://doi.org/10.1177/0363546510376053.
[12] Ardern CL, Taylor NF, Feller JA, Webster KE. Fifty-five per cent return to competitive sport following anterior cruciate ligament reconstruction surgery: an updated systematic review and meta-analysis including aspects of physical functioning and contextual factors. Br J Sports Med 2014;48(21):1543–52. https://doi.org/10.1136/bjsports-2013-093398.
[13] Ljungqvist O, Soop M, Hedström M. Why metabolism matters in elective orthopedic surgery: a review. Acta Orthop 2007;78(5):610–5. https://doi.org/10.1080/17453670710014293.
[14] Flück M, Viecelli C, Bapst AM, Kasper S, Valdivieso P, Franchi MV, et al. Knee extensors muscle plasticity over a 5-years rehabilitation process after open knee surgery. Front Physiol 2018:1343. https://doi.org/10.3389/fphys.2018.01343.

[15] Miljkovic I, Kuipers AL, Cauley JA, Prasad T, Lee CG, Ensrud KE, et al. Greater skeletal muscle fat infiltration is associated with higher all-cause and cardiovascular mortality in older men. J Gerontol A: Biomed Sci Med Sci 2015;70(9):1133–40. https://doi.org/10.1093/gerona/glv027.
[16] Snow BJ, Wilcox JJ, Burks RT, Greis PE. Evaluation of muscle size and fatty infiltration with MRI nine to eleven years following hamstring harvest for ACL reconstruction. JBJS 2012;94(14):1274–82. https://doi.org/10.2106/JBJS.K.00692.
[17] Reidy PT, McKenzie AI, Mahmassani Z, Morrow VR, Yonemura NM, Hopkins PN, et al. Skeletal muscle ceramides and relationship with insulin sensitivity after 2 weeks of simulated sedentary behaviour and recovery in healthy older adults. J Physiol 2018;596(21):5217–36. https://doi.org/10.1113/JP276798.
[18] Aburasayn H, Al Batran R, Ussher JR. Targeting ceramide metabolism in obesity. Am J Physiol Endocrinol Metab 2016;311(2):E423–35. https://doi.org/10.1152/ajpendo.00133.2016.
[19] Salaun E, Lefeuvre-Orfila L, Cavey T, Martin B, Turlin B, Ropert M, et al. Myriocin prevents muscle ceramide accumulation but not muscle fiber atrophy during short-term mechanical unloading. J Appl Physiol 2016;120(2):178–87. https://doi.org/10.1152/japplphysiol.00720.2015.
[20] Green CD, Maceyka M, Cowart LA, Spiegel S. Sphingolipids in metabolic disease: the good, the bad, and the unknown. Cell Metabol 2021;33(7):1293–306. https://doi.org/10.1016/j.cmet.2021.06.006.
[21] Tippetts TS, Holland WL, Summers SA. Cholesterol–the devil you know; ceramide–the devil you don't. Trends Pharmacol Sci 2021;42(12):1082–95. https://doi.org/10.1016/j.tips.2021.10.001.
[22] Marra F, Svegliati-Baroni G. Lipotoxicity and the gut-liver axis in NASH pathogenesis. J Hepatol 2018;68(2):280–95. https://doi.org/10.1016/j.jhep.2017.11.014.
[23] Lee SM, Lee SH, Jung Y, Lee Y, Yoon JH, Choi JY, et al. FABP3-mediated membrane lipid saturation alters fluidity and induces ER stress in skeletal muscle with aging. Nat Commun 2020;11(1):5661. https://doi.org/10.1038/s41467-020-19501-6.
[24] Lee WJ, Kim M, Park H-S, Kim HS, Jeon MJ, Oh KS, et al. AMPK activation increases fatty acid oxidation in skeletal muscle by activating PPARα and PGC-1. Biochem Biophys Res Commun 2006;340(1):291–5. https://doi.org/10.1016/j.bbrc.2005.12.011.
[25] Schrauwen-Hinderling VB, Hesselink MK, Schrauwen P, Kooi ME. Intramyocellular lipid content in human skeletal muscle. Obesity 2006;14(3):357–67. https://doi.org/10.1038/oby.2006.47.
[26] Burakiewicz J, Sinclair CDJ, Fischer D, Walter GA, Kan HE, Hollingsworth KG. Quantifying fat replacement of muscle by quantitative MRI in muscular dystrophy. J Neurol 2017;264(10):2053–67. https://doi.org/10.1007/s00415-017-8547-3.
[27] Wren TA, Bluml S, Tseng-Ong L, Gilsanz V. Three-point technique of fat quantification of muscle tissue as a marker of disease progression in Duchenne muscular dystrophy: preliminary study. AJR Am J Roentgenol 2008;190(1):W8–12. https://doi.org/10.2214/AJR.07.2732.
[28] Arnold DL, Taylor DJ, Radda GK. Investigation of human mitochondrial myopathies by phosphorus magnetic resonance spectroscopy. Ann Neurol 1985;18(2):189–96. https://doi.org/10.1002/ana.410180205.
[29] Yap JLY, Tai YK, Fröhlich J, Fong CHH, Yin JN, Foo ZL, et al. Ambient and supplemental magnetic fields promote myogenesis via a TRPC1-mitochondrial axis: evidence of a magnetic mitohormetic mechanism. Faseb J 2019;33(11):12853–72. https://doi.org/10.1096/fj.201900057R.
[30] Tai YK, Ng C, Purnamawati K, Yap JLY, Yin JN, Wong C, et al. Magnetic fields modulate metabolism and gut microbiome in correlation with Pgc-1α expression: follow-up to an in vitro magnetic mitohormetic study. Faseb J 2020;34(8):11143–67. https://doi.org/10.1096/fj.201903005RR.
[31] Vanhamme L, van den Boogaart A, Van Huffel S. Improved method for accurate and efficient quantification of MRS data with use of prior knowledge. J Magn Reson 1997;129(1):35–43.
[32] Sinclair CD, Samson RS, Thomas DL, Weiskopf N, Lutti A, Thornton JS, et al. Quantitative magnetization transfer in in vivo healthy human skeletal muscle at 3 T. Magn Reson Med 2010;64(6):1739–48. https://doi.org/10.1002/mrm.22562.
[33] Yarnykh VL. Actual flip-angle imaging in the pulsed steady state: a method for rapid three-dimensional mapping of the transmitted radiofrequency field. Magn Reson Med 2007;57(1):192–200. https://doi.org/10.1002/mrm.21120.
[34] Deoni SC, Rutt BK, Peters TM. Rapid combined T1 and T2 mapping using gradient recalled acquisition in the steady state. Magn Reson Med 2003;49(3):515–26. https://doi.org/10.1002/mrm.10407.
[35] Sinclair CD, Morrow JM, Hanna MG, Reilly MM, Yousry TA, Golay X, et al. Correcting radiofrequency inhomogeneity effects in skeletal muscle magnetisation transfer maps. NMR Biomed 2012;25(2):262–70. https://doi.org/10.1002/nbm.1744.
[36] Argov Z, Löfberg M, Arnold DL. Insights into muscle diseases gained by phosphorus magnetic resonance spectroscopy. Muscle Nerve 2000;23(9):1316–34. https://doi.org/10.1002/1097-4598(200009)23:9<1316::aid-mus2>3.0.co;2-i.
[37] Valkovic L, Chmelik M, Ukropcova B, Heckmann T, Bogner W, Frollo I, et al. Skeletal muscle alkaline Pi pool is decreased in overweight-to-obese sedentary subjects and relates to mitochondrial capacity and phosphodiester content. Sci Rep 2016;6:20087. https://doi.org/10.1038/srep20087.
[38] Hinkley JM, Cornnell HH, Standley RA, Chen EY, Narain NR, Greenwood BP, et al. Older adults with sarcopenia have distinct skeletal muscle phosphodiester, phosphocreatine, and phospholipid profiles. Aging Cell 2020;19(6):e13135. https://doi.org/10.1111/acel.13135.
[39] Hands LJ, Bore PJ, Galloway G, Morris PJ, Radda GK. Muscle metabolism in patients with peripheral vascular disease investigated by 31P nuclear magnetic resonance spectroscopy. Clin Sci (Lond) 1986;71(3):283–90. https://doi.org/10.1042/cs0710283.
[40] Suzuki E, Kashiwagi A, Hidaka H, Maegawa H, Nishio Y, Kojima H, et al. 1H- and 31P-magnetic resonance spectroscopy and imaging as a new diagnostic tool to evaluate neuropathic foot ulcers in Type II diabetic patients. Diabetologia 2000;43(2):165–72. https://doi.org/10.1007/s001250050025.
[41] Szendroedi J, Chmelik M, Schmid AI, Nowotny P, Brehm A, Krssak M, et al. Abnormal hepatic energy homeostasis in type 2 diabetes. Hepatology 2009;50(4):1079–86. https://doi.org/10.1002/hep.23093.
[42] Summermatter S, Santos G, Pérez-Schindler J, Handschin C. Skeletal muscle PGC-1α controls whole-body lactate homeostasis through estrogen-related receptor α-dependent activation of LDH B and repression of LDH A. Proc Natl Acad Sci USA 2013;110(21):8738–43. https://doi.org/10.1073/pnas.1212976110.
[43] Kuraoka M, Kimura E, Nagata T, Okada T, Aoki Y, Tachimori H, et al. Serum osteopontin as a novel biomarker for muscle regeneration in Duchenne muscular dystrophy. Am J Pathol 2016;186(5):1302–12. https://doi.org/10.1016/j.ajpath.2016.01.002.
[44] Wasgewatte Wijesinghe DK, Mackie EJ, Pagel CN. Normal inflammation and regeneration of muscle following injury require osteopontin from both muscle and non-muscle cells. Skeletal Muscle 2019;9(1):1–13. https://doi.org/10.1186/s13395-019-0190-5.
[45] Zhang T, Choi SJ, Wang Z-M, Birbrair A, Messi ML, Jin J-P, et al. Human slow troponin T (TNNT1) pre-mRNA alternative splicing is an indicator of skeletal muscle response to resistance exercise in older adults. J Gerontol A: Biomed Sci Med Sci 2014;69(12):1437–47. https://doi.org/10.1093/gerona/glt204.
[46] Oh K-J, Lee DS, Kim WK, Han BS, Lee SC, Bae K-H. Metabolic adaptation in obesity and type II diabetes: myokines, adipokines and hepatokines. Int J Mol Sci 2016;18(1):8. https://doi.org/10.3390/ijms18010008.
[47] Yan B, Shi X, Zhang H, Pan L, Ma Z, Liu S, et al. Association of serum irisin with metabolic syndrome in obese Chinese adults. PLoS One 2014;9(4):e94235. https://doi.org/10.1371/journal.pone.0094235.
[48] Sun Y, Gao H-Y, Fan Z-Y, He Y, Yan Y-X. Metabolomics signatures in type 2 diabetes: a systematic review and integrative analysis. J Clin Endocrinol Metab 2020;105(4):1000–8. https://doi.org/10.1210/clinem/dgz240.
[49] de Farias Costa PR, Kinra S, D'Almeida V, Assis AMO. Serum homocysteine and cysteine levels and changes in the lipid profile of children and adolescents over a 12-month follow-up period. Clin Nutr ESPEN 2017;21:13–9.
[50] Kaplan P, Tatarkova Z, Sivonova MK, Racay P, Lehotsky J. Homocysteine and mitochondria in cardiovascular and cerebrovascular systems. Int J Mol Sci 2020;21(20):7698.
[51] Holeček M. Histidine in health and disease: metabolism, physiological importance, and use as a supplement. Nutrients 2020;12(3):848.
[52] Zaitsev AV, Martinov MV, Vitvitsky VM, Ataullakhanov FI. Rat liver folate metabolism can provide an independent functioning of associated metabolic pathways. Sci Rep 2019;9(1):1–18.
[53] Perseghin G, Lattuada G, Danna M, Sereni LP, Maffi P, De Cobelli F, et al. Insulin resistance, intramyocellular lipid content, and plasma adiponectin in patients with type 1 diabetes. Am J Physiol Endocrinol Metab 2003;285(6):E1174–81.
[54] Ramirez-Camacho I, Bautista-Pérez R, Correa F, Buelna-Chontal M, Román-Anguiano N, Medel-Franco M, et al. Role of sphingomyelinase in mitochondrial ceramide accumulation during reperfusion. Biochim Biophys Acta, Mol Basis Dis 2016;1862(10):1955–63.
[55] Hooijmans M, Niks E, Burakiewicz J, Verschuuren J, Webb A, Kan H. Elevated phosphodiester and T2 levels can be measured in the absence of fat infiltration in Duchenne muscular dystrophy patients. NMR Biomed 2017;30(1):e3667.
[56] Bryant ND, Li K, Does MD, Barnes S, Gochberg DF, Yankeelov TE, et al. Multi-parametric MRI characterization of inflammation in murine skeletal muscle. NMR Biomed 2014;27(6):716–25. https://doi.org/10.1002/nbm.3113.
[57] Nuñez-Peralta C, Montesinos P, Alonso-Jiménez A, Alonso-Pérez J, Reyes-Leiva D, Sánchez-González J, et al. Magnetization transfer ratio in lower limbs of late onset pompe patients correlates with intramuscular fat fraction and muscle function tests. Front Neurol 2021;12:213.
[58] Hooijmans M, Doorenweerd N, Baligand C, Verschuuren J, Ronen I, Niks E, et al. Spatially localized phosphorous metabolism of skeletal muscle in Duchenne muscular dystrophy patients: 24–month follow-up. PLoS One 2017;12(8):e0182086.
[59] Arpan I, Forbes SC, Lott DJ, Senesac CR, Daniels MJ, Triplett WT, et al. T2 mapping provides multiple approaches for the characterization of muscle involvement in neuromuscular diseases: a cross-sectional study of lower leg muscles in 5–15-year-old boys with Duchenne muscular dystrophy. NMR Biomed 2013;26(3):320–8.
[60] Yao L, Gai N. Fat-corrected T2 measurement as a marker of active muscle disease in inflammatory myopathy. Am J Roentgenol 2012;198(5):W475–81.
[61] Varghese JS D Ono, Aneja C, Kay A, Ramam WA, Rajagopalan SV, Simonetti S, et al. Exercise induced changes in T1, T2 relaxation times and blood flow in the lower extremities in healthy subjects. J Cardiovasc Magn Reson 2013;15(1).
[62] Van Wessel T, De Haan A, Van der Laarse W, Jaspers R. The muscle fiber type–fiber size paradox: hypertrophy or oxidative metabolism? Eur J Appl Physiol 2010;110(4):665–94.
[63] Lepley LK, Davi SM, Burland JP, Lepley AS. Muscle atrophy after ACL injury: implications for clinical practice. Sport Health 2020;12(6):579–86. https://doi.org/10.1177/1941738120944256.
[64] Wong CJK, Tai YK, Yap JLY, Fong CHH, Loo LSW, Kukumberg M, et al. Brief exposure to directionally-specific pulsed electromagnetic fields stimulates extracellular vesicle release and is antagonized by streptomycin: a potential regenerative medicine and food industry paradigm. Biomaterials 2022;287:121658. https://doi.org/10.1016/j.biomaterials.2022.121658.

[65] Tai YK, Chan KKW, Fong CHH, Ramanan S, Yap JLY, Yin JN, et al. Modulated TRPC1 expression predicts sensitivity of breast cancer to doxorubicin and magnetic field therapy: segue towards a precision medicine approach. Front Oncol 2021:11. https://doi.org/10.3389/fonc.2021.783803.
[66] Parate D, Kadir ND, Celik C, Lee EH, Hui JHP, Franco-Obregón A, et al. Pulsed electromagnetic fields potentiate the paracrine function of mesenchymal stem cells for cartilage regeneration. Stem Cell Res Ther 2020;11(1):46. https://doi.org/10.1186/s13287-020-1566-5.
[67] Carroll TJ, Herbert RD, Munn J, Lee M, Gandevia SC. Contralateral effects of unilateral strength training: evidence and possible mechanisms. J Appl Physiol (1985) 2006;101(5):1514–22. https://doi.org/10.1152/japplphysiol.00531.2006.
[68] Hendy AM, Spittle M, Kidgell DJ. Cross education and immobilisation: mechanisms and implications for injury rehabilitation. J Sci Med Sport 2012;15(2):94–101. https://doi.org/10.1016/j.jsams.2011.07.007.
[69] Andrushko JW, Gould LA, Farthing JP. Contralateral effects of unilateral training: sparing of muscle strength and size after immobilization. Appl Physiol Nutr Metabol 2018;43(11):1131–9. https://doi.org/10.1139/apnm-2018-0073.
[70] Valdes O, Ramirez C, Perez F, Garcia-Vicencio S, Nosaka K, Penailillo L. Contralateral effects of eccentric resistance training on immobilized arm. Scand J Med Sci Sports 2021;31(1):76–90. https://doi.org/10.1111/sms.13821.
[71] Bilet L, Phielix E, van de Weijer T, Gemmink A, Bosma M, Moonen-Kornips E, et al. One-leg inactivity induces a reduction in mitochondrial oxidative capacity, intramyocellular lipid accumulation and reduced insulin signalling upon lipid infusion: a human study with unilateral limb suspension. Diabetologia 2020;63(6):1211–22. https://doi.org/10.1007/s00125-020-05128-1.
[72] Iotti S, Frassineti C, Alderighi L, Sabatini A, Vacca A, Barbiroli B. In vivo (31)P-MRS assessment of cytosolic [Mg(2+)] in the human skeletal muscle in different metabolic conditions. Magn Reson Imaging 2000;18(5):607–14.

Supplementary Information

Supplementary Tables

Supplemental Table 1: Baseline group demographics

Patient Demographics Table

	CON (n=10)	PEMF (n=10)
Age	24 (19-42)	25 (19-38)
No Males / Females	5 / 5	9 / 1
Leg operated [R / L]	6 / 4	3 / 7
MVC at baseline (operated leg)	46 ± 22	44 ± 17
MVC at baseline (unoperated leg)	61 ± 40	50 ± 18

Baseline clinical characteristics of the two groups.

Supplemental Table 2: CONSORT diagram and patient schedule

CONSORT diagram

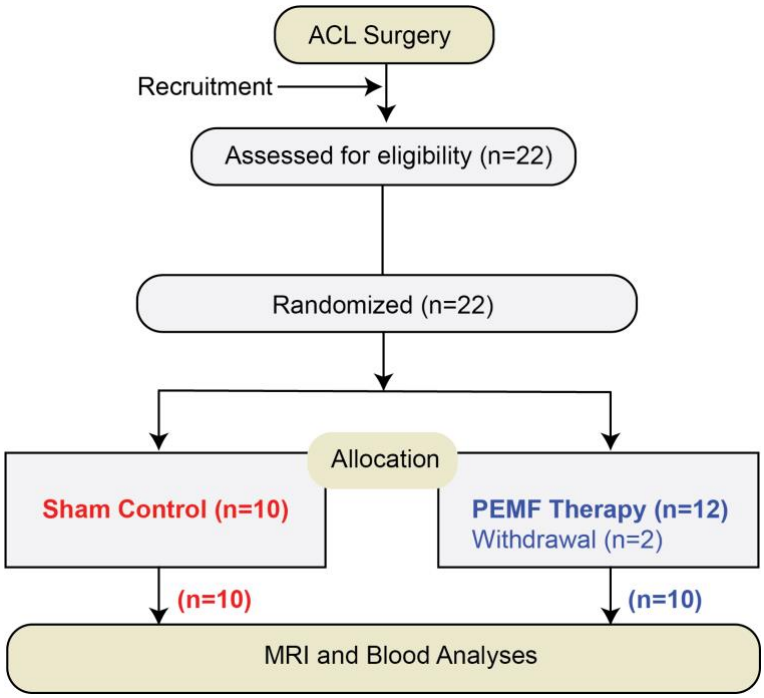

Patient Schedule:

Treatment			**Outcome Assessment**		
	Standard Rehab	Therapy PEMF/Sham	MRI	Blood Analysis	Clinical Scoring
Target	**Both Legs**		**Operated Leg**	**Systemic**	
Pre-surgery				✓	
Week 1	✓	✓	✓		
Week 2	✓	✓			
Week 3	✓	✓			
Week 4	✓	✓			
Week 5	✓	✓			
Week 6	✓	✓			
Week 7	✓	✓			
Week 8	✓	✓			
Week 9		✓			
Week 10	✓	✓			
Week 11		✓			
Week 12	✓	✓			
Week 13		✓			
Week 14	✓	✓			
Week 15		✓			
Week 16	✓	✓	✓	✓	✓

This study was conducted at the National University Health Systems (NUHS) of Singapore and authorized by the Domain Specific Review Board (DSRB) of the National Healthcare Group (NHG). 20 patients requiring ACL reconstruction were recruited into the study and were randomized into two groups (single-blind): Experimental cohort (n=10; age=25.9 [19-38], M/F=9/1) receiving PEMF therapy (10 min/week at 1 mT) on the operated (ACLR) leg and Control cohort (n=10; age=24.2 [19-42], M/F=5/5) who received sham exposure to operated leg.

Inclusion Criteria

The inclusion criteria were as follows: (1) age 18-50 years, (2) symptoms and a physical examination consistent with the diagnosis of ACL deficiency and magnetic resonance imaging results indicating ACL injury, (3) no contralateral ACL injury, (4) no previous surgeries in the

index knee, and (5) no other ligament reconstruction to be performed in the index knee (e.g. posterior cruciate ligament reconstruction or lateral tenodesis).

Supplemental Table 3: Plasma Biomarkers Analyzed by ELISA

Biomarker	Brand/Cat No.	Dynamic Range	Sample Volume
Human Osteopontin (OPN) Quantikine	R&D Systems/DOST00	0.313 - 20 ng/mL	*25-fold dilution of sample* 10 µl of plasma + 240 µl of Calibrator Diluent RD5-24, add 50 µl of diluted sample per well
Human Follistatin Quantikine	R&D Systems/DFN00	250 - 16,000 pg/mL	100 µl plasma/well
Human Troponin T Type 1, Slow Skeletal (TNNT1)	MyBioSource/MBS9307499	3.12 - 1,000 pg/mL	50 µl plasma/well
Human Procollagen Type III N-Terminal Propeptide (P3NP)	MyBioSource/MBS045955	3.12 - 100 ng/mL	50 µl plasma/well
Human Irisin	MyBioSource/MBS706887	3.12 - 200 ng/mL	100 µl plasma/well
Human Free Brain-Derived Neurotrophic Factor (BDNF) Quantikine	R&D Systems/DBD00	62.5 - 4,000 pg/mL	50 µl plasma/well (Additional centrifugation required: 10,000 g x 10 min at 4°C for complete platelet removal)
Human Pro-Cathepsin B Quantikine	R&D Systems/DCATB0	0.156 - 10 ng/mL	*20-fold dilution of sample* (10 µl of plasma + 190 µl of Calibrator Diluent RD5-34, add 50 µl of diluted sample per well)

Supplementary Table 4. LC-MS/MS MRM parameters such as the collision energy (CE), cell accelerator voltage (CAV), and polarity. The limits of quantification (LOQ) and linearity coefficients of determination R2 from linear standard curves for selected small molecule biomarkers and the corresponding internal standards (IS) were also shown. ND= not determined.

Metabolite	Transition	CE	CAV	Polarity	LOQ	R2

	m/z				(umol)	
Arginine	175 > 70	25	5	Positive	4.59	0.992858
Arginine IS	185.1 > 122.1	25	5	Positive	ND	ND
Phenylalanine	166 > 120	10	5	Positive	1.60	0.991177
Phenylalanine IS	176.1 > 129.1	10	5	Positive	ND	ND
Tyrosine	182 > 136	8	5	Positive	1.60	0.996861
Tyrosine IS	192.1 > 98.1	30	7	Positive	ND	ND
Isoleucine	132 > 69.1	19	5	Positive	3.24	0.998767
Isoleucine IS	139 > 74.1	20	5	Positive	ND	ND
Homocysteine	136.1 > 90.2	10	5	Positive	2.31	0.984808
Homocysteine IS	140.2 > 94.2	8	5	Positive	ND	ND
Cysteine	121.8 > 75.8	12	5	Positive	1.60	0.992806
Cystine IS	249 > 124.1	11	5	Positive	ND	ND
Methionine	150.1 > 104.1	15	5	Positive	1.60	0.985923
Methionine IS	156.2 > 109	15	5	Positive	ND	ND
Histidine	112.1 > 95	15	5	Positive	1.60	0.991177
Histidine IS	165.2 > 118.2	15	5	Positive	ND	ND

Supplemental Table 5: Changes in ^{31}P MR parameters at 16 weeks

Marker	Δ Control	*p*	Δ PEMF	*p*	Between groups
PCr/ATP	8.6 ± 12.0	0.082	3.5 ± 11.8	0.397	0.388
Pi/ATP	45.6 ± 33.3	0.006	16.6 ± 15.4	0.012	0.033
Pi/PCr	33.7 ± 24.3	0.006	13.7 ± 17.5	0.047	0.069
(Pi+PCr)/ATP	12.7 ± 13.2	0.030	4.8 ± 10.7	0.217	0.197
pH_{Sum} (abs)	-0.01 ± 0.04	0.507	0.03 ± 0.07	0.287	0.213
pH_{main} (abs)	-0.0004 ± 0.0190	0.951	0.0395 ± 0.0278	0.003	0.004
PME/PDE	-2.4 ± 58.9	0.911	21.0 ± 87.4	0.495	0.533
PME/ATP	14.4 ± 66.8	0.562	4.5 ± 81.1	0.873	0.786
PDE/ATP	18.9 ± 18.7	0.025	-13.9 ± 10.6	0.004	0.0004

Measured changes in ^{31}P MR parameters at 16 weeks (relative to baseline). Data are presented as mean ± SD % change from baseline.

Supplemental Table 6: Plasma Biomarkers Levels Determined by ELISA

Marker	Δ Control	*p*	Δ PEMF	*p*	*Between groups*
Osteopontin	21.7 ± 35.0	0.123	29.36 ± 34.9	0.049	0.669
TNNT1	6.8 ± 19.1	0.346	-14.3 ± 14.3	0.026	0.025

Follistatin	16.0 ± 30.7	0.184	31.3 ± 50.3	0.122	0.475
P3NP	4.9 ± 77.3	0.864	112.4 ±220.8	0.193	0.215
Irisin	64.1 ± 65.6	0.028	38.8 ± 66.8	0.175	0.474
Cathepsin-D	14.3 ± 25.3	0.155	6.15 ± 25.7	0.520	0.534
BDNF	9.60 ± 97.2	0.801	1.02 ± 58.55	0.965	0.844

Measured changes in plasma biomarkers detected by ELISA at 16 weeks (relative to baseline). Data are presented as mean ± SD % change from baseline.

Supplemental Table 7: Small molecule biomarkers detection by Liquid Chromatography with tandem Mass Spectrometry

Marker	Δ Control	*p*	Δ PEMF	*p*	*Between groups*
Allantoin	5.9 (-21.4 – 21.7)	1.000	-9.3 (-25.4 – 6.0)	0.461	0.641
Arginine	28.2 (15.1 – 47.5)	0.016	-5.0 (-38.7 – 7.6)	0.313	0.028
Cysteine	31.2 (17.6 – 40.4)	0.016	-16.8 (-23.8 - -6.6)	0.195	0.010
Histidine	13.3 (6.1 – 21.1)	0.039	-1.0 (-19.8 – 6.9)	0.742	0.130
Homocysteine	196.5 (-69.4 – 522.9)	0.195	-44.8 (-71.8 - -9.0)	0.008	0.442
Hypoxanthine	-0.34 (-31.8 – 98.4)	0.844	-59.5 (-66.0 - -33.7)	0.250	0.641
Isoleucine	18.9 (-10.4 – 39.6)	0.383	-21.3 (-27.1 – 17.3)	0.844	0.442
Lysine	7.8 (2.0 – 13.6)	0.078	-6.6 (-12.8 - -1.4)	0.250	0.050
Methionine	16.5 (11.0 – 59.0)	0.023	-25.4 (-45.6 – 5.5)	0.383	0.028
Phenylalanine	16.6 (7.8 – 63.1)	0.078	-6.5 (-24.4 – 6.4)	0.313	0.021
Proline	9.9 (-2.4 – 30.9)	0.195	7.8 (-29.5 – 26.0)	0.844	0.645
Tyrosine	347 (274-418)	0.023	408 (285 – 554)	0.945	0.053
Uric acid	8.4 (-0.8 – 18.2)	0.250	-6.5 (-18.0 – 7.9)	0.313	0.109
Xanthine	29.6 (12.8 – 580.2)	0.078	12.3 (-35.5 – 52.6)	0.844	0.505

Measured changes in small molecule biomarkers detected by Liquid Chromatography with tandem mass spectrometry at 16 weeks (relative to baseline). Data are presented as median (interquartile) % change from baseline.

Supplemental Table 8 : MRI muscle volumes and fat fractions

Marker	Δ Control	*p*	Δ PEMF	*p*	*Between groups*
Muscle Volumes					
Total Muscle	4.5 ± 9.0	0.1	0.8 ± 8.9	0.8	0.4

AM	51.0 ± 64.7	0.046	29.2 ± 37.2	0.4	0.5
BLH	15.2 ± 8.2	0.0002	18.3 ± 27.1	0.003	0.7
BSH	7.5 ± 21.8	0.3	-1.9 ± 6.9	0.06	0.2
Grac	-44.6 ± 30.1	0.001	-73.6 ± 33.6	0.4	0.1
RF	10.8 ±16.9	0.1	-3.7 ± 37.1	0.003	0.4
Sart	3.7 ± 10.7	0.3	8.9 ± 14.3	0.9	0.4
SM	1.3 ± 7.0	0.6	5.0 ± 13.3	0.08	0.4
ST	-23.6 ± 36.0	0.2	-21.8 ± 38.1	0.2	0.9
VI	-3.5 ± 7.5	0.2	-8.3 ± 18.7	0.2	0.5
VL	4.9 ± 18.7	0.4	6.1 ± 23.4	0.4	0.9
VM	22.2 ± 32.3	0.06	1.5 ± 23.1	0.8	0.1
Fat					
SC fat	14.5 ± 17.5	0.03	14.2 ± 11.9	0.005	1.0
AM	-0.5 ±8.5	0.8	6.3 ± 14.6	0.2	0.2
BLH	-3.0 ± 8.4	0.3	4.6 ±11.3	0.2	0.1
BSH	4.2 ± 7.4	0.1	8.1 ± 8.8	0.02	0.3
Grac	33.5 ± 28.7	0.005	63.0 ± 39.6	0.0007	0.07
RF	1.0 ± 14.3	0.8	13.1 ± 17.4	0.04	0.1
Sart	6.0 ± 13.6	0.2	14.8 ±18.9	0.04	0.2
SM	2.6 ± 6.1	0.2	6.5 ±11.8	0.1	0.4
ST	19.5 ± 19.5	0.01	32.2 ± 14.8	0.00007	0.1
VI	7.1 ± 6.8	0.009	11.3 ±8.8	0.003	0.2
VL	1.9 ± 11.3	0.6	2.0 ± 3.8	0.1	1.0
VM	-3.4 ± 14.9	0.5	6.1 ± 8.3	0.04	0.09

Measured changes in muscle volumes and fat fractions from MRI. Measured values are presented as mean ± SD.

Supplemental Table 9 : Quantitative Magnetization Transfer measurements.

Marker	**Δ Control**	***p***	**Δ PEMF**	***p***	***Between groups***
$T1_{obs}$	1.0 ± 12.0	0.8	5.1 ± 7.1	0.046	0.4
f_pc	2.6 ± 15.2	0.6	-1.6 ± 6.8	0.5	0.4

T_2^A	1.4 ± 12.9	0.8	6.1 ± 8.5	0.048	0.4
R/g	-6.7 ± 8.8	0.05	-7.4 ± 14.4	0.1	0.9
MTR	3.6 ± 4.0	0.03	4.8 ± 5.4	0.02	0.6

Measured changes in MTR values from the quadriceps. Measured values are presented as mean ± SD.

Supplementary Figure 1.

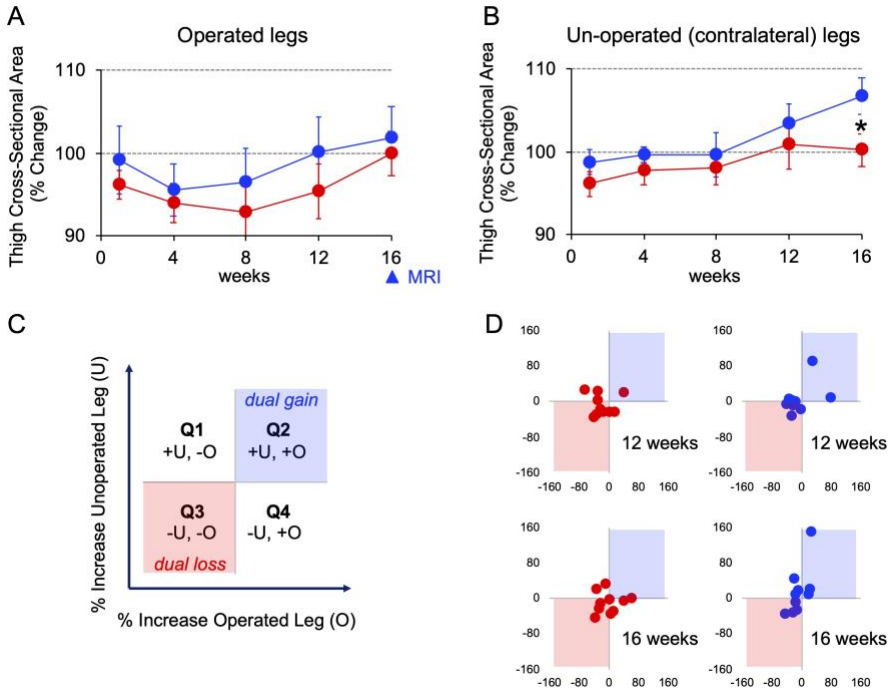

Supplementary Figure 1. Thigh cross-sectional areas (**A**, **B**) and dynamometer power output (**C**, **D**) in the operated and unoperated (contralateral) legs at the indicated time points after ACLR. **A**) Thigh cross-sectional areas for the operated legs of the experimental (**blue**) and sham control (**red**) cohorts. **B**) Thigh cross-sectional areas for the unoperated (contralateral) legs of the experimental (**blue**) and sham control (**red**) cohorts. Leg volume normalize by 16 weeks (**blue arrowhead**), when MRI assessment was made post-ACLR. A significant increase in thigh cross-sectional area was observed in the contralateral limbs of the experimental cohort of at week 16. **C**) Schematic explanation of (**D**), whereby improvements in strength of the contralateral leg would be seem as shifts to quadrants 1 and 2 (Q1, Q2) and improvements in strength of the operated leg would be seem as shifts to quadrants 2 and 4 (Q2, Q4); strength gains in both would be depicted as shifts to Q2 and losses of strength in both legs would be reflected by shifts to Q3. **D**) Changes in dynamometer power output for the operated and unoperated legs at the indicated time points as explained in panel **C**. **Blue** symbols represent those subjects receiving magnetic intervention; **red** symbols the sham control cohort. Thigh circumference measurements were made by a licensed physical therapist. The data were analysed using two-sample paired t-test with *$p < 0.05$ and the error bars represent the standard error of the mean. N=10 for control group and N=10 for PEMF group.

Supplementary Methods

Detailed Surgical Procedure

The graft was prepared by first placing whipstitches at both ends of each tendon with nonabsorbable sutures (Ultrabraid). The gracilis and semitendinosus tendons were then looped around a nonabsorbable suture (Ethibond Exel No. 5) to form a quadrupled hamstring graft. Ultrabraid sutures were then used to reinforce the femoral and tibial segments of the graft. The tibial tunnel was drilled at the center of the ACL footprint. The femoral tunnel was drilled at the anatomic anteromedial bundle position through the anteromedial portal with the knee in 120 degrees of flexion. After the creation of the femoral and tibial tunnels, the leading suture of the graft (Ethibond Exel No. 5) was pulled through the tibial tunnel and then into the femoral tunnel. After the passage of the graft through the tibial and femoral tunnels, it was fixed at the femoral tunnel with a bioabsorbable interference screw (Biosure, Smith & Nephew). The graft was then tensioned with the knee in slight flexion before fixation at the tibial tunnel with another bioabsorbable interference screw (Biosure). Concomitant meniscal injury was treated with either meniscal repair or partial meniscectomy as indicated intraoperatively. The tibial tunnel was drilled at the center of the ACL footprint. The femoral tunnel was drilled at the anatomic anteromedial bundle position through the anteromedial portal with the knee in 120 degrees of flexion. After the creation of the femoral and tibial tunnels, the leading suture of the graft (Ethibond Exel No. 5) was pulled through the tibial tunnel and then into the femoral tunnel. After the passage of the graft through the tibial and femoral tunnels, it was fixed at the femoral tunnel with a bioabsorbable interference screw (Biosure, Smith & Nephew). The graft was then tensioned with the knee in slight flexion before fixation at the tibial tunnel with another bioabsorbable interference screw (Biosure). Concomitant meniscal injury was treated with either meniscal repair or partial meniscectomy as indicated intraoperatively.

Blood Collection

Participants were asked to fast for at least 12 hours for pre-surgery and post-intervention blood draws prior to any other trial-related procedure. Peripheral blood (12 mL) was collected from the antecubital vein and stored in K_2EDTA tubes (lavender cap; BD #366643, Canada). The procedure was conducted by a licensed phlebotomist or equivalent (e.g. SAF-certified army medic/ nurse). Immediately after collection, the tubes were gently inverted 8 times and transported on ice. The blood samples were next centrifuged at 2000 x g (10min, 4°C) and the plasma transferred to 1.7 mL microcentrifuge tube (Axygen #MCT-175-C, USA) and kept on ice until storage at -80°C.

Analysis of Plasma for LC-MS/MS

A 50µL aliquot of plasma was mixed with 50µL of internal standard and after treating with 360µL of ice-cold Acetonitrile containing 0.1% Formic acid, the plate was mixed on a shaker at 1000 rpm/min for 10 minutes, then centrifuged down at 2270*g* for 50 minutes at 4°C. 140µL of the supernatant was carefully transferred to a 96-microwell plate and loaded into the auto-sampler for analysis by LC-MS/MS.

LC-MS/MS Analysis

Liquid chromatographic (LC) separation of these biomarkers was performed using the SeQuant®ZIC®-cHILIC 3mm, 100Å 100 x 2.1 mm HPLC column (Merck Pte Ltd, Singapore) maintained at 40°C. The organic solvent was Acetonitrile containing 0.1% Formic acid (Solvent A) and the aqueous solvent used was 20 mM Ammonium Formate pH 4.0 (Solvent B). A linear LC gradient on Binary Pump (Agilent Model G7120A) was set up with a percentage of Solvent B as follows: 10% at 0 minutes, 70% at 9.00 minutes, 70% at 11.0 minutes, and 10% between 11.1 and 11.5 minutes, with a flow rate of 0.4 mL/min. The

column was further equilibrated for further 11.5 minutes with 10% Solvent B. An additional high-speed pump, Binary Pump B (Agilent Model G7120A), together with a Quick-Change valve head, 2-position/10-port, 1,300 bar (Agilent Part No: 5067-4240), were utilized to reduce the cycle times by automated alternating column regeneration. % of Solvent B on Binary Pump B was maintained at 10% with a flow rate of 0.4 mL/min. The sample injection volume was 5μL.

For mass detection, the LC eluent is connected online to an Agilent 6495 Triple Quadrupole MS system (Instrument model G6495A, Agilent Technologies) operated with the electrospray source in negative ionization mode. The electrospray ionization source conditions were as follows: capillary voltage of 4.0 kV, nozzle voltage of 500 V, ion funnel parameter high/low-pressure RF of 90V, nebulizer pressure of 35psi, the gas temperature of 290°C, sheath gas temperature of 350°C, and sheath gas flow of 12 L/min. Acquisitions and quantitative analysis were performed using the Agilent MassHunter Workstation Acquisition (10.0.127) and Agilent MassHunter Workstation Quantitative Analysis (10.0) software.

Power Calculation

The method of sample size calculation used in this study was based on inequality Tests for two Means using Differences (Two-Sample T-Test). The primary outcome used in this study was muscle volume, which will be continuous measures with percentages. A change of approximately 20% increase at the end of the study period is set to be clinically important in this study. We assumed that the conservative mean muscle volume in the intervention (i.e. device) group and control group (i.e. standard of care) will be 30.0 and 10.0. We also assumed that conservative common standard deviation (SD) in intervention and control group will be 17.0 and 12.0 respectively. We also set a level of significance of 5% and a power of 80%, a minimum sample size of 20 subjects (ie. 10 per group) will be required for this study. Further,

assuming an attrition rate of 10%, the anticipated sample size is 22 (i.e. 11 per group). We also set a level of significance of 5% and power of 80%. The hypothesised values used in these calculations were based on published literature [1,2], as well as the opinions from the technical and clinical experts, as well as in-house pilot experimental data with conservative anticipated estimates.

Muscle Strength Measurements

Muscle force was assessed using a seated dynamometer (TKK-5710e Tension Meter and TKK5715 Chair Assembly; TAKEI Scientific Instruments Co., LTD, Niigata, Japan). Subjects were advised to push against the pedal, in a short burst, and to the maximum of their ability. This was repeated 5 times and the peak value was taken as the Maximum Voluntary Contraction (MVC).

References

1. Charles D, White R, Reyes C, Palmer D. A Systematic Review of the effects of blood flow restriction training on quadriceps muscle atrophy and circumference post ACL rescontruction. Int J Sports Phys Ther 2020;15(6):882-91 Doi:10.26603/ijspt20200882.

2. Lepley LK, Davi SM, Burland JP, Lepley AS. Muscle Atrophy After ACL Injury: Implications for Clinical Practice. Sports Health 2020;12(6):579-86 Doi:10.1177/1941738120944256.